

I.1 Scientific Motivation

I.1.1 The Heavy Ion Physics Program

I.1.1.a Soft Physics

Measurements of Global E_T

The most interesting collisions at RHIC are those that produce the highest densities and temperatures. This is thought to be the most promising environment in which to search for novel phenomena and signatures of a deconfined phase of quarks and gluons. The most characteristic feature of these conditions is expected to be the observation at mid-rapidity of a high multiplicity of particles and high transverse energy deposition (E_T).

The distribution of E_T characteristically observed in relativistic nuclear collisions consists of a plateau region followed by a region of rapidly decreasing probability at the highest E_T values as shown in Fig I.1.1-1¹. The slope of the distribution in the high E_T region is determined by fluctuations in the energy-transferring interactions of the nuclear constituents. It has been suggested that a measurable part of these fluctuations may be due to fluctuations in the partonic states of the incident hadronic systems², and are interesting for this reason. Whatever their origin, the fluctuations in E_T represent variations in the energy density produced in the collisions and must be measured accurately if that range of energy densities is to be understood.

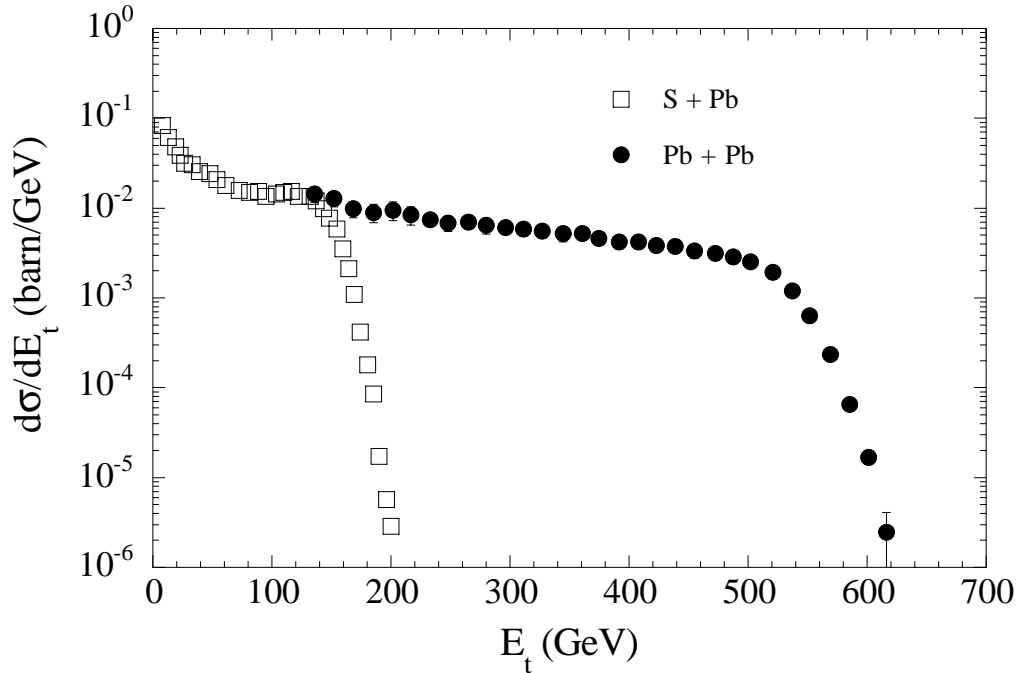


Figure I.1.1-1. The distribution of E_T observed by NA49¹ for 158 GeV/nucleon S + Pb and Pb + Pb collisions for $2.1 < \eta < 3.4$. The distribution exhibits a plateau followed by a region of rapidly decreasing probability at the highest E_T values.

¹ T. Alber et al. (NA49), Phys. Rev. Lett. **75**, 3814 (1995).

² B. Blättel et al., Nucl. Phys **A544** (1992) 479.

Experimental resolutions that are comparable to, or larger than, the natural physics width of the parent distribution lead to a dilution of the sample of high E_T events and are therefore undesirable. With the proposed barrel electromagnetic calorimeter, which is the only device that measures E_T (as opposed to multiplicity), the resolution for determining E_T improves to $\sim 2\%$, such that $\sim 90\%$ of the events in the top 5% of the observed distribution will originate from the parent distribution of interest. The parent distribution is assumed to have an intrinsic width of $\sigma = 5\%$. This is comparable, for example, to the results obtained for S+Pb collisions at 200 A GeV with the Helios³ spectrometer. In this instance, the experimental resolution was $\sigma = 3.8\%$, and the observed E_T falloff of 7% could be interpreted in terms of physical processes.

Searching for Rare Events Indicating a Phase Transition

It has been argued^{4,5,6} on rather general grounds for some time that the mean transverse momentum, $\langle p_T \rangle$, of particles produced in hadronic interactions, observed as a function of the multiplicity

$$N = \int (dN/dy) dy \quad (\text{I.A-1})$$

in a given rapidity interval, reflects the properties of the equation of state of high temperature hadronic matter. Assuming that a description in terms of hydrodynamics is appropriate, dN/dy is related to the entropy, whereas the p_T spectrum reflects the combined effects of temperature and transverse expansion. Except in the vicinity of a phase transition, higher entropy production in normal hadronic matter requires higher temperature, a correlation observed experimentally, for example, at the CERN collider.⁷ In the vicinity of a first order phase transition however, the large latent heat required to melt the hadronic matter into a plasma of quarks and gluons leads to a situation in which the energy density and entropy density may increase dramatically, while the temperature and pressure remain essentially constant. In this instance one would expect to observe a departure from the usual correlation between dN/dy and $\langle p_T \rangle$ in which the increase in the mean p_T as a function of multiplicity slowed, or even decreased slightly due to reduced transverse expansion in a limited range of dN/dy . Above the transition, one would again recover the standard correlation, the thermodynamic relations for an ideal gas of massless quarks and gluons being similar to that for a gas of massless pions. The behavior one might expect to observed experimentally is indicated qualitatively in Fig. I.1.1.-2.

While this picture suffers from a number of oversimplifications, more detailed studies⁸ of the hydrodynamic evolution of matter in ultrarelativistic nucleus-nucleus collisions appear to indicate the behavior expected based on the simple arguments presented above survives the refinement of proper treatment of the longitudinal and

³T. Akesson et al., Nucl. Phys. **B353** (1991) 1.

⁴E.V. Shuryak, Phys. Rep. **61** (1980) 71.

⁵E.V. Shuryak and O. Zhirov, Phys. Lett. **89B** (1980) 253; Sov. J. Nucl. Phys. **28** (1978)247.

⁶L. Van Hove, Phys. Lett. **118B** (1982) 138.

⁷UA1 Collaboration, G. Arnison et al., "Transverse Momentum Spectra for Charged Particles at the CERN Proton-Anti-proton Collider," presented XXIth International Conference on High Energy Physics, July 1982, Paris, France.

⁸M Kataja, P.V. Ruuskanen, L.D. McLerran, and H. von Gersdorff, Phys. Rev. **D34** (1986) 2755.

transverse expansion which occur during the mixed phase. The mean p_T in this instance does not decrease in any interval of dN/dy , although the increase in the vicinity of the phase transition is once again slowed considerably (Fig. I.1.1.-3). Perhaps the most important conclusion however, is that the correlation between $\langle p_T \rangle$ and dN/dy does in fact reflect properties of the equation of state. While the order and nature of the transition are matters for experiment, the sensitivity of this correlation to the fundamental character of the matter being probed makes this correlation potentially a useful tool in identifying events in which a transition has occurred.

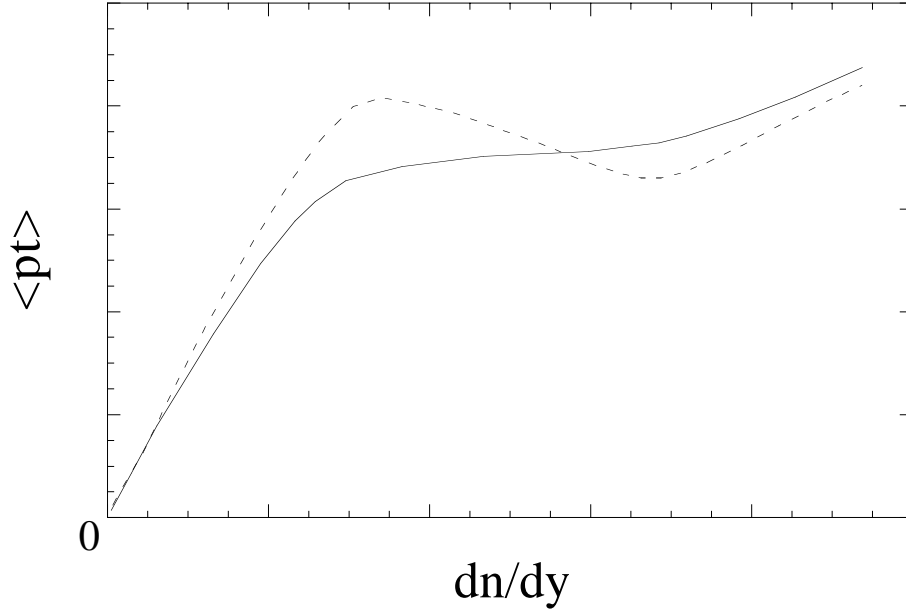


Figure I.1.1-2. The expected structure in the $\langle p_T \rangle$ versus dn/dy correlation at a given impact parameter resulting from a first order phase transition. Further details may be found in Reference 6.

If the transition to a plasma of quarks and gluons occurs with high probability, the correlation between $\langle p_T \rangle$ and dn/dy is best studied within STAR using single particle inclusive data provided by the time projection chamber (TPC). Aside from possible Coulomb effects which should be small, there is no reason to expect a priori that the mean p_T measured for charged pions should be different than that for π^0 's. In that event, the resolution and systematic uncertainties in determining the mean $\langle p_T \rangle$ using tracks in the TPC will be better than can be obtained by reconstructing low momentum π^0 's in the EMC, although some account will need to be taken of the fact that charged pions having $p_T < 40$ MeV/c spiral in the magnetic field and do not reach the TPC. The effective p_T cutoff may in fact be somewhat higher in nucleus-nucleus collisions due to the high occupancy for the inner pad rows, although the silicon vertex tracker (SVT) will in principle recover most low momentum tracks. Use of the TPC tracking would in any event be preferable for studying this correlation since it would provide the most precise minimum bias data.

If the transition to the deconfined phase is rare however, it will be necessary, due to the overhead in analyzing large data samples, to develop a highly selective trigger to identify such events. Since complete tracking information from the TPC will not be available at the trigger level, the TPC alone can not provide such a trigger. If the

correlation between $\langle p_T \rangle$ and dN/dy were known to be similar to that in Fig. I.1.1-3, for example, this could be accomplished simply by using the STAR central trigger barrel (CTB) to search for events with a given dN/dy . In reality however, the correlation between $\langle p_T \rangle$ and dN/dy is completely unknown even for normal events in this energy range. In practice therefore, one would establish the behavior of the correlation for normal events, and then develop a trigger to search for a sample of events exhibiting an unusual correlation between $\langle p_T \rangle$ and dN/dy . Since such events might occur as fluctuations in a normal range of dN/dy , the most exhaustive search would be conducted by examining the correlation between $\langle p_T \rangle$ and dN/dy at the trigger level, rather than triggering on multiplicity alone.

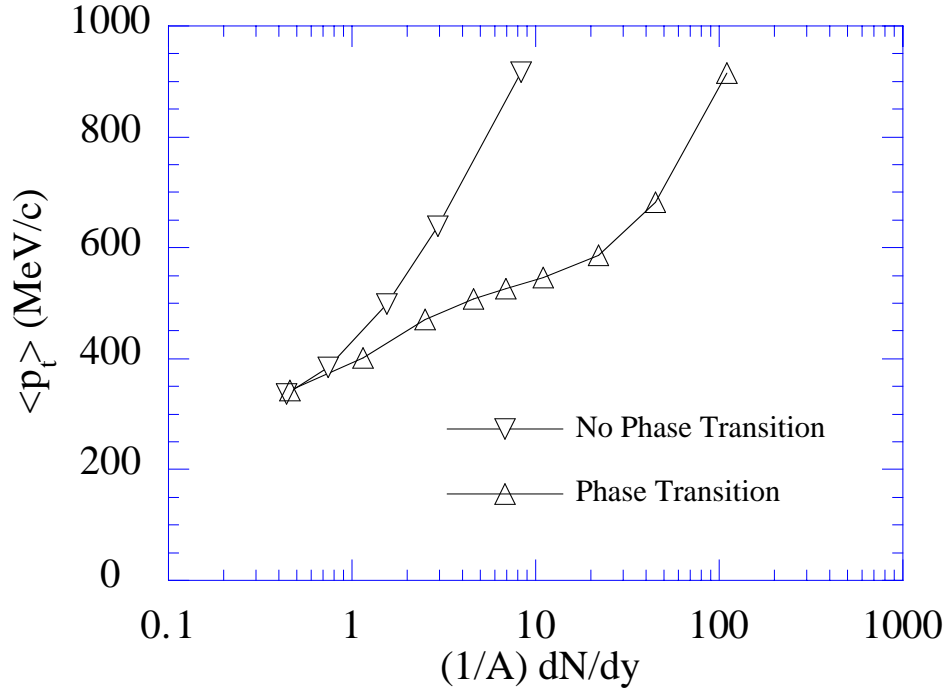


Figure I.1.1-3. The prediction from Reference 8 for the average p_T as a function of the normalized multiplicity $(1/A) dN/dy$ with (Δ) and without (∇) a first order phase transition. At the point indicated by $\epsilon = \epsilon_o$, pure plasma state at T_c is reached.

The STAR EMC provides a useful means to test this correlation at the trigger level. Because the calorimeter is sensitive to the ionization energy loss of charged particles as well as that from electromagnetic showers, the STAR EMC is sensitive to changes in the mean p_T in a given event. When correlated with the multiplicity information provided by the STAR CTB on an event-by-event basis, or by using the EMC multiplicity information (available at higher levels of the trigger) the EMC provides a unique capability in STAR to search for events with an unusual correlation between energy density and entropy density. If such events are rare, the use of this highly selective trigger may be the only means by which to observe them.

Isospin Fluctuations and Chiral Symmetry Restoration

A number of conjectures have recently been put forward suggesting that one may expect large fluctuations in the photon to hadron ratio in ultra-relativistic heavy ion collisions. The interest in such possibilities stems from the apparent observation of large fluctuations in this ratio in recent cosmic ray data.⁹⁻¹⁰ Although the physical bases for these predictions vary, all depend upon the high density and temperature that can be reached in central nucleus-nucleus collisions at RHIC.

Panagiotou et al.¹¹ consider that, assuming isospin is conserved, the low number of photons from π^0 decay observed in cosmic ray emulsion data may result from ultra-relativistic nucleus-nucleus collisions in which all pion production is suppressed in a given interval of rapidity. This is noted to be possible if a quark-gluon fireball with non-zero net baryon number is formed, since the high baryochemical potential in such a state suppresses the thermal production of quarks and anti-quarks and therefore the production of pions as well. A fireball of this type would most likely appear in the fragmentation region at RHIC and would be characterized by the suppression of all pion species. A related observation would be that baryons produced in the decay of the fireball would be characterized by a higher than average $\langle p_T \rangle$.

A somewhat less speculative hypothesis by Pratt¹² expands on an earlier possibility suggested by Anselm and Ryskind¹³ that a coherent pion field may be produced. More precisely, when the density of possible emission sources of identical bosons within a given volume exceeds a certain critical density, quantum interference effects and symmetrization of the N-body wave function become important. The consequence of symmetrization may be striking. In particular, stimulated emission of pions into low momentum states (pion lasing) might result. The multiplicity of pions is enhanced in general with large fluctuations in the number of pions of a given species possible, due to the fact that the interference depends upon the indistinguishability of bosons of a given isospin. This prediction is especially relevant for π^0 production where the unknown effects of Coulomb interactions are not a consideration. As a consequence, instead of a low photonic to hadronic ratio, one might expect some events to exhibit "anti-Centauro" behavior, with π^0 decay photons greatly outnumbering the charged pions observed in a limited region of rapidity ($|\Delta y| < 1$). Empirical estimates from S + Pb collisions at CERN suggest that the pion densities reached are within a factor of two of the critical density required for stimulated emission, and that in any event, this effect will need to be accounted for in order to understand high-multiplicity events. An enhancement of the observed pion spectra at low p_T , and two-particle HBT correlations indicating coherent production would be other indications that symmetrization was important.

Taking a deeper look at the QCD vacuum, Bjorken¹⁴ suggests that a collision between two ultra-relativistic heavy ions may result in a highly excited, colorless system whose isospin orientation may be quite arbitrary. As a consequence, the ratio of neutral to charged pions may fluctuate widely from the normal isospin expectation. Bjorken

⁹Chacaltaya and Pamir Collaboration, Tokyo University preprint ICRR Report-232-91-1 (1991).

¹⁰C.M.G. Lattes, Y. Fugimoto, and S. Hawegawa, Phys. Rep. **65** (1980) 151.

¹¹A. Panagiotou et al., Phys. Rev. **D45** (1991) 3134.

¹²S. Pratt, Phys. Lett. **B301** (1993) 159.

¹³A.A. Anselm and M. Pyskind, Phys. Lett. **B266** (1991) 482.

¹⁴J.D. Bjorken, Acta Physica Polonica **B23** (1992) 637.

expects that heavy ions may be the most effective way to produce this phenomenon. This prediction is similar to that of Wilczek¹⁵, who suggests that a disoriented chiral condensate may be one consequence of a quench of the quark-gluon plasma which may be formed.

Investigation of these phenomena depends entirely on the ability to identify neutral electromagnetic energy (π^0 daughters) and charged particles over a wide range of acceptance. This study is therefore not possible in STAR without the capabilities provided by the electromagnetic calorimeter. The TPC and charged-particle multiplicity detectors together with the proposed EM calorimeter can accomplish this task with reasonable spatial and energy resolution. The potential for discovery of such wide fluctuations in the photon to hadron ratio is therefore a distinct possibility. Simulations designed to determine the limits of the ability of the EM calorimeter to identify, trigger upon, and measure these fluctuations are described in elsewhere in this report. The results indicate clearly, that with the coverage projected in the STAR EMC proposal, a sensitive search for these exciting possibilities in heavy ion collisions at RHIC is feasible.

1.1.1.B. High p_T , Hard Probes, and Parton Physics

Parton Energy Loss

The measurement of jets, direct photons, electrons from heavy flavor and quarkonium decays, and high p_T particles using the STAR electromagnetic calorimeter is essential, since these processes presently represent the only means within STAR of probing the high temperature, gluon-dominated, pre-equilibrium stage of the collision. A goal of studying the products of hard QCD processes in relativistic heavy ion collisions is to use the propagation of quarks and gluons as a penetrating probe of nuclear matter, hot hadronic matter, and quark matter. Since the hard-scattering processes occur at the very earliest stage of the collision ($t < 1$ fm/c), their production rates are dependent only upon the incoming state. Given the quark and gluon structure functions of the colliding nuclei, the rate as a function of p_T of hard parton scattering is entirely calculable using perturbative QCD. This situation is unique to RHIC, which will be the first accelerator to provide nuclear collisions at energies where rates of detectable partonic debris (jets, high- p_T particles, and direct photons) from hard partonic scattering permit accurate measurements.

Various calculations have predicted that the propagation of quarks and gluons through matter depends strongly upon properties of the medium,¹⁶⁻¹⁷⁻¹⁸⁻¹⁹⁻²⁰ and that a measurement of the yield of hard-scattered partons as a function of transverse energy may be sensitive to the state of the surrounding matter. It has been suggested, for example, that there will be observable changes in the energy loss of propagating partons as the energy density of the medium increases, particularly if the medium passes through

¹⁵F. Wilczek, "Chiral Dynamics Near Equilibrium or After Quenching," Proceedings of the Tenth International Conference on Ultra-Relativistic Nucleus-Nucleus Collisions, June 20–24, 1993, Borlänge, Sweden.

¹⁶J.D. Bjorken, Fermilab Report 82/59/59-THY (1982).

¹⁷D. Appel, Phys. Rev. **D33** (1986) 717.

¹⁸J.P. Blaizot and L.D. McLerran, Phys. Rev. **D34** (1986) 2739.

¹⁹M. Rammersdorfer and U. Heinz, Phys. Rev. **D41** (1990) 306.

²⁰M. Gyulassy and M. Plummer, Phys. Lett. **B243** (1990) 432.

a phase transition to the QGP.²¹ Interest in this possibility originally focused on the observation that the collisional energy loss of a quark of energy E propagating through an ideal plasma of quarks and gluons at temperature T could be expressed²² as

$$(dE/dx) \propto \alpha_s^2 T^2 \log(4ET/M^2) \exp(-M/T) (1 + M/T) , \quad (\text{I.A-2})$$

where M is an infrared cutoff on the order of the Debye mass. The strong dependence of this expression on α_s lead to speculation that in the vicinity of a phase transition the normal energy loss experienced by propagating quarks and gluons might be reduced due to decreased coupling between partons in this environment. More recently, it has been noted²³ that another sensitive probe may be the radiative energy loss of propagating partons,

$$(dE/dx) \propto \alpha_s M^2 (\log(s/4M^2))^2 . \quad (\text{I.A-3})$$

whereas the radiative energy loss for high-energy partons propagating through nuclear matter would normally be strongly suppressed due to the Landau-Pomeranchuk effect, the reduced Debye screening length predicted²⁴ for the plasma ($\lambda_D = M^{-1} \sim 0.4$) could increase the radiative energy loss significantly. This same effect is predicted to lead to the suppression of vector meson production (J/ψ , ψ' , Υ) Correlation of these results could help determine if effects that might be observed for vector meson production are due to plasma formation, or result instead from propagation within the nuclear medium.

The consequence of parton energy loss in a medium is jet quenching, or the reduction of the jet yield at a given p_T . This effect, which is most important for intermediate energy jets (5-10 GeV), has already been observed in deep inelastic lepton scattering from nuclear targets.²⁵ It is most effectively studied using the $qg \leftrightarrow qg$ Compton subprocess, since for this process complications due to the fragmentation function are not a consideration and the p_T of the parton scatter may be determined from the p_T of the direct photon, modulo k_T smearing of the p_T balance from initial state radiation of the quarks and gluons. (An effect measurable from diphoton production in $p+A$ collisions)

It may also be studied using di-jets. In this instance it is essential to measure the energy of both jets in di-jet events. The sum of the jet energies and the di-jet invariant mass are sensitive to interactions of the partons with the medium. The yield as a function of invariant mass of back-to-back jets at mid-rapidity may be the best tool for studying effects of the matter on propagation, since in this case the overall path length in the medium is maximized. The difference of di-jet energies may be sensitive to the

²¹M. Gyulassy et al., Lawrence Berkeley Laboratory Report LBL-31002, to be published in Proceedings of 4th Conference on the Intersections between Particle and Nuclear Physics, Tucson, Arizona, 1991.

²²J.D. Bjorken, Fermilab Report 82/59/59-THY (1982).

²³M. Gyulassy, "Nuclear Chromodynamics in eA, pA, and AA Interactions," proceedings of the Future Directions in Particle and Nuclear Physics at Multi-GeV Hadron beam Facilities Meeting, March 4-6, 1993, Brookhaven National Laboratory, Upton, New York.

²⁴B. Muller, "Physics of the Quark-Gluon Plasma," Proceedings of the NATO Advanced Study Institute on Particle Production in Highly Excited Matter, July 12-24, 1992, Il Ciocco, Italy; Duke Report No. DUKE-TH-92-36

²⁵L. S. Osborne et al., Phys. Rev. Lett. **40** (1978) 1624; P.B. Renton et al., Oxford Nuclear Physics Laboratory preprint 55/88 (1988); M Gyulassy and M. Plummer, LBL preprint LBL-27234.

difference in path lengths traversed by the partons. In addition, measurement of both jets in a di-jet event suppresses background due to fluctuations of soft production processes that can mimic a jet. A measurement of the di-jet differential cross section for p-nucleus collisions will in itself be of interest for understanding the parton structure functions in nuclear matter.

Jet quenching is also expected to lead to significant effects in the spectra of single high p_T particles, di-hadrons, and jets in AA collisions at RHIC.²⁶ This is not surprising since virtually all particles observed above $p_T \sim 2\text{--}3$ GeV/c arise as fragmentation products from hard parton scatters.

In general, the reconstruction of the parton-scattering kinematics is limited by acceptance and detector resolution effects, and by the superposition of particles from other, incoherent processes which occur during the collision. This last problem is especially serious in high-multiplicity AA collisions, where the jet can be entirely obscured. The technique of jet reconstruction to extract parton information with the STAR EMC in pA and AA collisions is presently being investigated. Nonetheless, because the heart of any jet identification algorithm is the correlations between nearby particles, the ability to measure photons as well as high p_T charged particles is an important element in any jet reconstruction program. The yield of jets as a function of p_T , as well as the ability of the STAR EMC to trigger upon jets is discussed further elsewhere in this report.

A systematic study of parton energy loss in pA and AA interactions using the STAR EMC will provide a unique tool to search for a transition to a quark gluon plasma in ultra-relativistic nucleus-nucleus collisions. Additionally, events identified as candidates for further study using other signatures may be probed with this technique to determine the nature of the medium in the initial phase of the collision. The STAR EMC is essential for this study of jets and direct photons, since measurement of the neutral electromagnetic energy is necessary to reconstruct jets or detect direct photons. Although the study of single high p_T particles may in principle be accomplished using tracking information from the STAR TPC, without the EMC it is not presently possible to trigger upon high p_T particles. Additionally, energy resolution as measured in a calorimeter improves with increasing energy, while momentum resolution as measured in a spectrometer degrades with increasing momentum.

Mini-Jets and High p_T Tails of Distributions

Mini-jets are expected to be produced copiously in collisions at RHIC.^{27,28} As is the case for high p_T jets, the observed yield of mini-jets is expected to be influenced strongly by the state of the high-density medium through which they propagate.²⁹ However, direct measurement of mini-jets is virtually impossible because of their large opening angle and the strongly varying background. Thus, it is important to study the degree of fluctuation of the transverse energy and multiplicity as a function of pseudo-rapidity and azimuthal angle ($d^2 E_T / d\eta d\phi$ and $d^2 n / d\eta d\phi$) event-by-event, which should be

²⁶X.N. Wang and M. Gyulassy, Phys. Rev. Lett. **68** (1992) 1480.

²⁷K. Kajantie, P.V. Landshoff, and J. Lindfors, Phys. Rev. Lett. **59** (1987) 2527.

²⁸K.J. Eskola, K. Kajantie, and J. Lindfors, Nucl. Phys. **B323** (1989) 37.

²⁹P.V. Landshoff, Nucl. Phys. **A498** (1989) 217; X.N. Wang, Lawrence Berkeley Laboratory Report LBL-28790 (1990), submitted to Phys. Rev. **D**.

strongly affected by the mini-jets.³⁰⁻³¹ The STAR EMC is essential for this study since without measuring the neutral transverse energy, the true degree of fluctuation due to mini-jets can not be determined. It is essential that this be systematically studied in pp and pA collisions, as well as AA.

Inclusive p_T distributions of hadrons at $p_t > 3$ GeV/c will also be influenced by jets and mini-jets. It should be emphasized that the single particle cross sections fall off more rapidly as a function of p_T than the jet cross sections.³² However, Wang and Gyulassy³³ have shown that the inclusive single particle yield is very sensitive to the state of the matter through which the parent scattered partons propagate. Figure I.1.1.-4 shows the charged particle pseudorapidity distribution and the ratio of charged particle yields for Au-Au and p-Au collisions compared to p-p collisions as a function of p_T , under various assumptions about the nuclear structure functions (shadowing) and energy loss of the scattered partons (quenching). From the middle panel of Fig. I.1.1.-4, it is seen that the introduction of quenching (in addition to shadowing) leads to a reduction in yield above $p_t \sim 4$ GeV/c of a factor 5. Although effects of this magnitude may be observed by examining single particle inclusive spectra provided by the TPC, unfolding the effects of shadowing and quenching in order to interpret these data will require systematic studies using the STAR EMC.

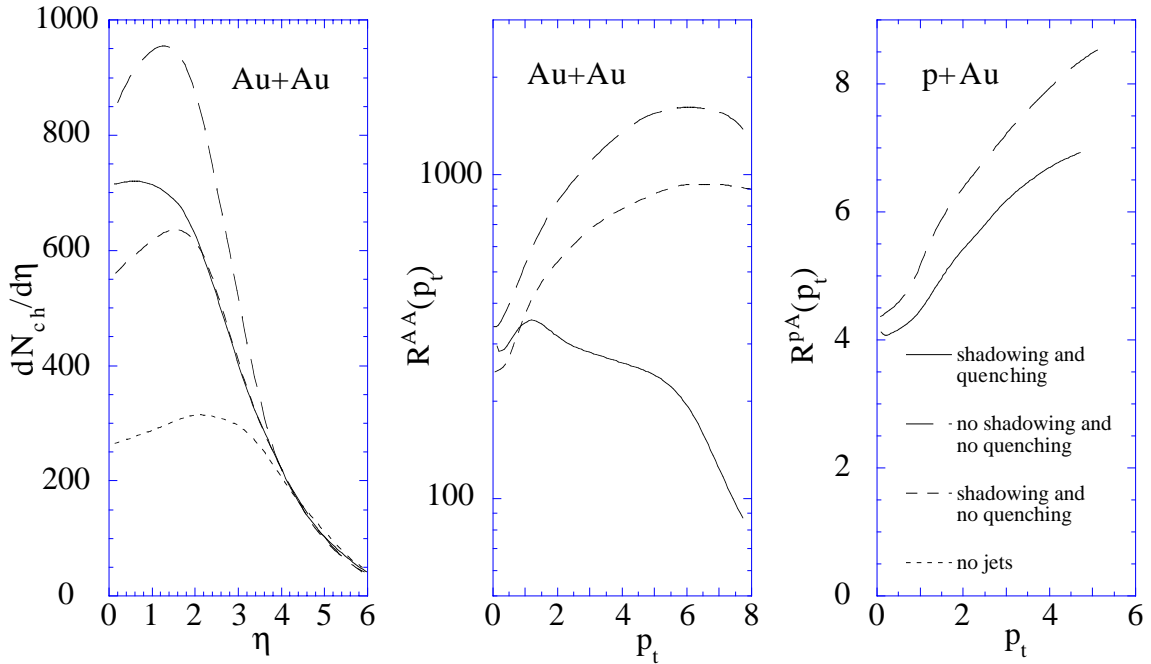


Figure I.1.1-4. Results from HIJING calculations on the dependence of the inclusive charged hadron spectra in central AuAu and pAu collisions on mini-jet production (dash-dotted), gluon shadowing (dashed) and jet quenching (solid) assuming that gluon shadowing is identical to that of quarks. $R^{AB}(p_t)$ is the ratio of the inclusive p_t spectrum of charged hadrons in A+B collisions to that of pp. Details may be found in Reference 33 in this chapter.

³⁰D. Appel, Phys. Rev. **D33** (1986) 717.

³¹X.N. Wang, Lawrence Berkeley Laboratory Report LBL-28789 (1990), submitted to Phys. Lett. B.

³²See W. Geist et al., CERN/EP Report 89-159 (1989) to be published in Phys. Rep. (1990).

³³X.N. Wang and M. Gyulassy, Phys. Rev. Lett. **68** (1992) 1480.

Gluon Shadowing

One of the primary advantages of RHIC is that unlike the situation at lower energy, where only a phenomenological approach was possible, firm predictions as to the early stages of the collision are possible using perturbative QCD. The ability to make full use of this potential, however, depends upon having knowledge of the parton structure functions in the nucleus. Deep inelastic scattering measurements presently underway will provide the necessary measurements for determination of the quark structure functions in nuclei, but little is expected to be known concerning the nuclear structure function for gluons at low Bjorken x . Simulations of the early stage of ultra-relativistic nucleus-nucleus collisions indicate it is precisely gluons at low Bjorken x which make the largest contribution to the energy density of the system produced at mid-rapidity, and dominate this phase of the evolution. The manifestation of this phase may be striking, including a dramatic increase in the production of open charm and mini-jets from semi-hard gluon-gluon scatters. Mini-jet production may account for up to 50% of the total transverse energy observed at mid-rapidity. Without measurement of the gluon shadowing, however, the theoretical predictions for dn_{ch}/d , and $d^2n/dydp_{\perp}$ are uncertain by $\sim 30\%$. The interpretation of these data will be much less certain, and the understanding seriously compromised, if the incident gluon flux has not been determined. Some information on the gluon structure function will be provided by the NMC experiment at CERN, and Fermilab experiments E665, E706, E772, and E789. The available data in the low- x region of interest ($0.01 < x < 0.05$) tends to be limited either by systematics or low statistics. STAR, however, can measure the gluon densities in nuclei by measuring jet and direct photon production in pA collisions. Again the $qg \leftrightarrow qg$ and $qg \leftrightarrow q\gamma$ Compton subprocess dominate here. These measurements in pA collisions are at exactly the same rapidity and p_T (or, equivalently, Bjorken x) as we are interested in for AA, further reducing the systematic uncertainties.

I.1.2 The Spin Physics Program

After decades of being regarded as an inessential complication to the strong interaction at high energy, spin has again come to the attention of the theoretical and experimental community. This is largely due to the fact that recent results from deep inelastic scattering experiments have shown that the spin of the nucleon is not accounted for by the spin of the quark constituents.^{34,35} A NLO fit to the available data indicates that $\Delta\Sigma$, the spin component of the nucleon carried by the light quarks, is $0.27 \pm 0.04 \pm \text{systematic}$ experimental and theoretical uncertainty³⁶. For the spin of the nucleon,

$$\frac{1}{2} = \frac{1}{2} \Delta\Sigma + \Delta G + L_z \quad (\text{I.1.2-1})$$

Since only one-fourth of the nucleon spin comes from the quark spins, the spin must be carried by the gluon field, ΔG , or by the orbital angular momentum L_z .

This nucleon spin anomaly has generated several theoretical explanations. In the chiral soliton model, spin arises from the coherent rotation of a meson cloud and ΔG is expected to be near zero³⁷. Single spin inclusive meson production using 200 GeV/c polarized proton and anti-proton beams has been interpreted in terms of quark-antiquark annihilation processes suggesting the existence of orbiting valence quarks inside polarized protons.³⁸ In theory based on the axial U (1) anomaly, ΔG is taken as a NLO correction to Δu , Δd , and Δs , and ΔG is expected to be large and positive³⁹. Spin distribution functions have recently been published which extract $\Delta G(x)$ from scaling violations in the existing data for Δu and Δd ⁴⁰. These generally predict moderate values for ΔG with $0 < \Delta G < 1$, but $\Delta G(x)$ can take on negative values for some range of x . There is also a theory that attempts to associate ΔG with the correct term in the momentum tensor for QCD and predicts $\Delta G < 0$ ⁴¹.

There is also an abundance of data showing large and inexplicable spin effects at relatively low values of transverse momenta. Some of these effects have been studied: the polarization of inclusively produced hyperons, as well as the analyzing power in pion production persist at the highest energies and transverse momenta. Experiments with polarized hadron (and also polarized lepton) beams have been limited to fixed target energies of a few hundred GeV. Perhaps these hadronic spin effects are low energy, low p_t phenomena, which will vanish at higher energies. On the other hand, perhaps they are asymptotic properties of the strong interaction. Continuing these measurements to very high energies would give much-needed answers. In fact, with a complete understanding of QCD and the spin structure of the proton, the spin effects observed in proton-proton collisions at RHIC energies should be calculable.

³⁴J. Ashman *et al.*, Phys. Lett. B206 (1988) 364; Nucl. Phys. B328 (1989) 1.

³⁵B. Adeva *et al.*, Phys. Lett. B302 (1993) 533. D.L. Adams *et al.*, Phys Lett B **336** (1994) 125; Phys Lett B **339** (1994) 332.

³⁶J. Ellis, hep-ph/9611208.

³⁷S.J. Brodsky, J. Ellis, and M. Karliner, Phys. Lett. B **206**, 309 (1988). J. Ellis and M. Karliner, Phys Lett B **313** (1993) 131; Phys Lett B **341** (1995) 397.

³⁸C. Boros, Liang Zuo-tang and Meng Ta-chung, Phys. Rev. Lett. **70** (1993) 1751.

³⁹A.V. Efremov and O.V. Teryaev, Dubna report JIN-E2-88-287 (1988); G. Altarelli and G. Ross, Phys. Lett. B **212**, 391 (1988); R.D. Carlitz, J.D. Collins and A.H. Mueller, Phys. Lett B **214**, 219 (1988).

⁴⁰M. Gluck *et al.*, hep-ph/9508347; T Gehrmann and W.J. Stirling, hep-ph/9512406; R.D. Ball, S. Forte, and G. Ridolphi, Phys. Lett. B **378**, 255 (1996).

⁴¹R.L. Jaffe, hep-ph/9509279.

A critical ingredient in these calculations is the spin distribution of the various constituents of the proton: valence, sea quarks, and gluons. The helicity distributions of the valence plus sea quarks in the proton and the neutron have been measured in deep inelastic scattering of longitudinally polarized muons and electrons from longitudinally polarized proton (deuteron) targets at CERN and SLAC. The separate helicity distributions of sea quarks and gluons and the transversity distribution of quarks are also fundamental properties of the proton that cannot be measured in lepton scattering, but can easily be measured at RHIC with polarized proton beams. Knowledge of the quark and gluon spin distribution is essential information for calculation of spin observables in various parton-parton scattering processes, e.g., dijet production and W^\pm and Z^0 production. All spin observables in $pp \rightarrow \text{jet} + \text{jet} + X$ should then be calculable, beginning at Q^2 values where higher twist effects must be included and extending out to Q^2 where only leading twist should be important. These measurements can easily be made at RHIC and afford stringent tests of QCD and of current models of the nucleon. Measurement of parity-violating asymmetries in weak boson production can further test the standard model and probe for new physics.

Measurement of all of the spin structure functions of the proton (quark, gluon, helicity, and transversity) at polarized RHIC would constitute a significant and important physics program.^{42,43,44,45} These structure functions could then be used to make detailed tests of QCD by measurement of spin asymmetries in hadronic scattering processes, which would allow the most detailed test of QCD and our understanding of the nucleon that have ever been made. The addition of the EMC would not only increase the capability of STAR for searching for the quark-gluon plasma (QGP) but also afford complementary tests of QCD at modest cost.

I.1.2.a. Status of Present Knowledge

Experimental programs using polarized beams and polarized targets at high energies have been active during the past three decades. Many asymmetry measurements in a number of scattering processes (e.g., elastic scattering, deep inelastic scattering, and inclusive meson production) have been carried out at various laboratories in the world. As unique measurements often bring surprises, many exciting and unexpected results in hadron-hadron and muon-nucleon scattering have been observed using polarized beams and targets. These include large spin effects in pp elastic scattering,^{46,47,48} inclusive pion production,^{49,50,51,52,53,54,55,56,57} and in p production.⁵⁸ The importance of spin as a funda-

⁴²C. Bourrely, J.Ph. Guillet, and J. Soffer, Nucl. Phys. **B361** (1991) 72.

⁴³M.A. Doncheski, F. Halzen, C.S. Kim, and M.L. Stong, University of Wisconsin report MAD/PH/744 (1993).

⁴⁴For a review of spin physics possible at RHIC, see proceedings of the Polarized Collider Workshop, AIP Conference Proceedings No. 223, University Park, PA, 1990.

⁴⁵G. Bunce *et al.*, Particle World **3** (1992) 1.

⁴⁶R.V. Kline *et al.*, Phys. Rev. **D22** (1980) 553.

⁴⁷G. Fidecaro *et al.*, Phys. Lett. **105B** (1981) 309.

⁴⁸F.Z. Khari *et al.*, Phys. Rev. **D39** (1989) 45.

⁴⁹L. Dick *et al.*, Phys. Lett. **57B** (1975) 93.

⁵⁰R.D. Klem *et al.*, Phys. Rev. Lett. **36** (1976) 929.

⁵¹D. Aschman *et al.*, Nucl. Phys. **B142** (1978) 220.

⁵²W.H. Dragoset *et al.*, Phys. Rev. **D18** (1978) 3939.

⁵³J. Antille *et al.*, Phys. Lett. **94B** (1980) 523.

⁵⁴S. Saroff *et al.*, Phys. Rev. Lett. **64** (1990) 995.

mental degree of freedom has also been observed experimentally in deep inelastic lepton scattering^{59,60} and hyperon production.^{61,62,63,64,65,66} Thus far, experiments with polarized proton beams have been limited to about 200 GeV/c. It is extremely important to explore spin effects at much higher energies where high p_t phenomena as well as parity-violating asymmetries in W^\pm and Z^0 production can be studied.

Programs to test quantum chromodynamics and explore the electroweak coupling at CERN and Fermilab have provided a wealth of information on the standard model of particle physics. However, these experiments at high-energy colliders do not cover the area of spin physics. Tests involving the spin-dependence in fundamental scattering processes such as jet, direct photon, Drell-Yan, and W^\pm , Z^0 boson production are yet to be carried out.

Polarized proton-proton collisions have previously been limited to a relatively low range of \sqrt{s} and Q^2 . Large polarization effects have been seen in many different experiments. Because of the low Q^2 , spin physics has been relegated to a soft physics compartment in high energy physics since interpretation of these data using QCD has been problematic. A comprehensive program of spin physics experiments at RHIC using the STAR EMC would allow measurement of the spin-dependent parton distributions of the proton (both longitudinal and transverse) and would provide fundamental spin tests of QCD and the electro-weak interaction. The high energy and luminosity at RHIC will permit experiments in which an interpretation in terms of perturbative QCD will be unambiguous.

I.1.2.b The Gluon Spin Distribution of the Proton

In this and subsequent sections, we present estimates of the acceptance of STAR and expected event rates for several reactions of interest.

In general, the luminosity at RHIC for pp running is energy dependent. The integrated luminosities used to calculate event rates discussed below are: $\int \ell dt = 800 \text{ pb}^{-1}$ at $\sqrt{s} = 500 \text{ GeV}$, assuming $\ell = 2 \times 10^{32} \text{ cm}^{-2} \text{ sec}^{-1}$, and $\int \ell dt = 320 \text{ pb}^{-1}$ at $\sqrt{s} = 200 \text{ GeV}$, assuming $\ell = 8 \times 10^{31} \text{ cm}^{-2} \text{ sec}^{-1}$. The beam polarization is assumed to be 0.7. The assumed running time is 10 weeks at 67% efficiency, or $4 \times 10^6 \text{ sec}$.

Information on the gluon spin distribution in polarized protons can be obtained by measuring asymmetries in the cross section for various scattering processes which depend on the helicities of the colliding beams. Such processes include inclusive direct- γ production, inclusive jet production, direct- γ + jet, and jet-jet coincidences. Inclusive di-

⁵⁵V.D. Apokin *et al.*, Phys. Lett. **243B** (1990) 461.

⁵⁶B.E. Bonner *et al.*, Phys. Rev. Lett. **61** (1988) 1918.

⁵⁷D.L. Adams *et al.*, Phys. Lett. **261B** (1991) 201; Phys. Lett. **264B** (1991) 462; Z. Phys. **C56** (1992) 181.

⁵⁸S. Heppelmann *et al.*, Phys. Rev. Lett. **55** (1985) 1824.

⁵⁹J. Ashman *et al.*, Phys. Lett. **B206** (1988) 364; Nucl. Phys. **B328** (1989) 1.

⁶⁰B. Adeva *et al.*, Phys. Lett. **B302** (1993) 533.

⁶¹G. Bunce *et al.*, Phys. Rev. Lett. **36** (1976) 1113.

⁶²S. Erhan *et al.*, Phys. Lett. **82B** (1979) 301.

⁶³B.E. Bonner *et al.*, Phys. Rev. **D38** (1988) 729.

⁶⁴L.G. Pondrom, Phys. Rep. **127** (1985) 57 and references therein.

⁶⁵B. Lundberg *et al.*, Phys. Rev. **D40** (1989) 3557.

⁶⁶K.B. Luk *et al.*, Phys. Rev. Lett. **70** (1993) 900.

rect- γ and direct- γ + jet production in pp interactions are dominated by a single parton-level subprocess,

$$q + g \rightarrow \gamma + q, \quad (\text{I.1.2-2})$$

and determining the spin-dependent gluon distribution of the proton from these processes is straightforward. On the other hand, inclusive jet and jet-jet production contain contributions from many parton-level subprocesses (e.g., gg, qq, qg, etc. scattering), and extraction of the spin-dependent gluon structure function using these processes is more difficult, despite their increased cross section. Consider the hadronic reaction, $pp \rightarrow (\text{hadron or gauge boson}) + X$. When both initial protons are longitudinally polarized with polarization P , we measure an observable A_{LL} defined as,

$$A_{LL} = (1/P^2)(N^{++} - N^{+-})/(N^{++} + N^{+-}), \quad (\text{I.1.2-3})$$

where N^{+-} , for example, is the yield observed when the helicities of the two colliding beams are anti-aligned. If one QCD subprocess is dominant, then

$$A_{LL} \approx P_a P_b \hat{a}_{LL(a+b \rightarrow c+d)}, \quad (\text{I.1.2-4})$$

where P_a and P_b are the polarizations of partons a and b in the proton, and A_{LL} is the parton-level asymmetry for a given subprocess.

For the determination of the gluon spin distribution, measurements of direct- γ , direct- γ with away-side jet, inclusive jet, and dijet production are proposed.

Direct- γ Production⁶⁷

Direct photons are produced through $q\bar{q}$ annihilation and the q - g Compton subprocess ($q + g \rightarrow \gamma + q$.) The Compton process is the dominant one in pp interactions at mid-rapidity since there are no valence antiquarks in the proton. Then,

$$A_{LL} \approx \left\langle \left[\Delta u(x_1)/u(x_1) \right] \cdot \left[\Delta G(x_2)/G(x_2) \right] \cdot \hat{a}_{LL(qg \rightarrow \gamma q)} \right\rangle \quad (\text{I.1.2-5})$$

where the u quark polarization is $\Delta u(x)/u(x) = [u_+(x) - u_-(x)]/[u_+(x) + u_-(x)]$, $\Delta u(x)$ is the u quark helicity distribution, and x is Bjorken x , the momentum fraction carried by the parton. Similarly, the gluon polarization is $\Delta G(x)/G(x) = [G_+(x) - G_-(x)]/[G_+(x) + G_-(x)]$, and $\Delta G(x)$ is the helicity distribution carried by gluon fields. The average in Eq. (I.1.2-5) is taken over the allowed kinematic range for the outgoing quark jet.

From deep inelastic scattering measurements, for example, $\Delta u(x)/u(x) \sim 0.4$ for $x_q \sim 0.2$. For the Compton process, $A_{LL} \sim 0.6$ at $\theta = 90^\circ$ in the parton center of mass frame. Consequently,

$$A_{LL} \approx 0.2 \times \frac{\Delta G}{G} \quad (\text{I.1.2.6})$$

and the uncertainty in the gluon polarization is related to the uncertainty in the measured asymmetry by

$$\delta \frac{\Delta G}{G} \approx 5 \times \delta A_{LL} \quad (\text{I.1.2-7})$$

With the proposed STAR barrel electromagnetic calorimeter ($|\eta| < 1$), using 1.5-cm-wide segmentation for the shower maximum detector, the estimated uncertainty in the measured asymmetry for $10 \text{ GeV}/c < p_t < 20 \text{ GeV}/c$ is

⁶⁷ M.E. Beddo, H. Spinka, and D.G. Underwood, ANL-HEP-TR-92-59, STAR Note 77 (1992).

$$\delta \frac{\Delta G}{G} \approx \pm 0.006 \sqrt{\frac{800 \text{ pb}^{-1}}{\int \ell dt}} \quad (\text{I.1.2-8})$$

at $\sqrt{s} = 500 \text{ GeV}$; at $\sqrt{s} = 200 \text{ GeV}$,

$$\delta \frac{\Delta G}{G} \approx \pm 0.03 \sqrt{\frac{320 \text{ pb}^{-1}}{\int \ell dt}} \quad (\text{I.1.2-9})$$

Direct- γ Production with Away-Side Jet Detection

In order to measure the x dependence of the gluon helicity distribution, $\Delta G(x)$, both the direct- γ and the away-side jet must be detected in coincidence so that the kinematics of the incoming partons can be calculated. For the STAR barrel EMC, it is possible to study γ -jet events in which $-0.3 < \eta_{\text{jet}} < 0.3$ and $-1.0 < \eta_{\gamma} < 1.0$. (With corrections for missing acceptance, it may be possible to extend the coverage for jets to $|\eta_{\text{jet}}| \leq 0.7$.) Jets will be reconstructed in STAR using the EM calorimeter to measure the electromagnetic component and the TPC to detect charged particles.⁶⁸ In the calculations, it was assumed that particles within a cone of radius $\sqrt{(\Delta\eta)^2 + (\Delta\phi)^2} = 0.7$ were part of the jet. The dominant process is $u + G \rightarrow u + \gamma$ and the longitudinal double spin asymmetry A_{LL} is approximately proportional to the product

$$\frac{\Delta u}{u}(x_1) \frac{\Delta G}{G}(x_2) + (x_1 \leftrightarrow x_2). \quad (\text{I.1.2-10})$$

For a u quark in the range $0.1 < x < 0.4$, the polarization is known experimentally to be large, $\frac{\Delta u}{u}(x) > x$.

We define a kinematic region for the measurement with $p_t > 10 \text{ GeV}/c$ and include jets (cone $R = 0.7$) in the rapidity range $-0.3 < \eta < 0.3$ (1.3) (endcap) and γ 's in the range $-1 < \eta < 1$ (2). For this region the scale of asymmetry is given by $A_{LL} \approx \text{constant} \times \frac{\Delta G}{G}$. The constant comes from a weighted integration of u quark polarization multiplied by parton level analyzing power and is typically 0.1 to 0.3 depending on kinematic cuts.

Because the gluon structure function is strongly peaked at $x < 0.1$ and the u quark polarization grows with x for $x > 0.1$, it is clear that asymmetric jet-direct photon detection requires the full rapidity coverage available in STAR. The expected errors in $\frac{\Delta G}{G}(x)$ from direct photon + jet events are shown in Fig. I.1.2-1.

The cutoff in data at small x results in the limits imposed by beam energy, minimum p_t , and the ratio x_1/x_2 (rapidity range). The best small x measurement comes from the highest energy pp running, $\sqrt{s} = 500 \text{ GeV}$. It is clear, that if lower p_t data could be interpreted, the region $x < 0.02$ would produce a very large number of events.

⁶⁸ B.Christie and K. Shesternanov, ANL-HEP-TR-95-11, STAR Note 196 (1995).

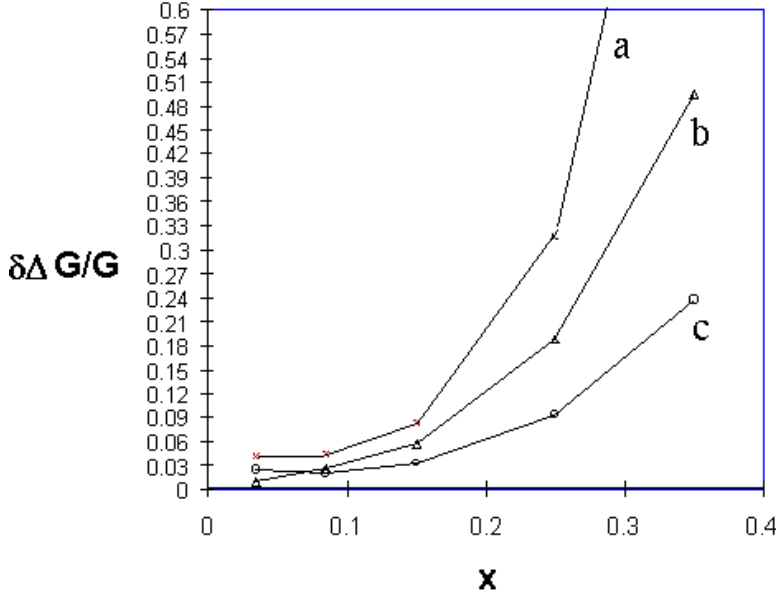


Figure I.1.2-1. Measurement error in $\Delta G/G$ vs. x for direct photon + jet events. Curve (a) represents errors for $\sqrt{s} = 500$ GeV with an EMC barrel only, curve (b) represents $\sqrt{s} = 500$ GeV with an EMC barrel + endcap.

Single-Jet Production

Several QCD subprocesses contribute to the cross section for jet production:

- Gluon-gluon scattering at low p_t ($gg \rightarrow gg$)
- Gluon-quark scattering at medium p_t ($gq \rightarrow gq$), and
- Quark-quark elastic scattering at high p_t ($qq \rightarrow qq$)

At low p_t , gluon-gluon scattering is expected to be the largest contribution to inclusive jet production, and to first order, therefore,

$$A_{LL} = [\Delta G(x_1)/G(x_1)] \times [\Delta G(x_2)/G(x_2)] \times \hat{a}_{LL(gg \rightarrow gg)} \quad (I.1.2-11)$$

where A_{LL} is ~ 0.8 for scattering at 90° in the parton cm frame. Because the cross section for inclusive jet production is large, ~ 200 nb for $E_T \text{ jet} > 15$ GeV at $\sqrt{s} = 500$ GeV, error on A_{LL} from a few weeks at very low luminosity is $\delta A_{LL} \approx 0.005$. This most elementary measurement at STAR will discriminate among the different theoretical models and place a large constraint on the parameterization of ΔG .

Dijet Production

When two back-to-back jets are detected, the kinematics of the incoming partons can be reconstructed to within a small correction that depends upon their intrinsic p_t . The reconstructed value of x for each parton may then be used to compute the parton-level subprocess asymmetry, A_{LL} . The measured value of A_{LL} then determines the parton polarization. Thus, dijet production may be used to provide an independent measurement of $\Delta G(x)$. Since several QCD subprocesses contribute to the cross section for jet production, and the relative importance of each varies with the kinematic region which is studied, it is more complicated to extract the gluon polarization $\Delta G(x)$ from dijet production than from direct- γ + jet production. However, since the cross section for dijet production is ~ 20 times greater than for direct- γ + jet production, the increased statistics could offset the larger systematic uncertainties of this method.

The cross section for back-to-back jets in the barrel is ~ 60 nb. Given about three months running at $\approx 10^{31} \text{ cm}^{-2}\text{s}^{-2}$ (50 pb^{-1}), STAR can measure $\Delta G/G(x)$ in the range $0.07 < x < 0.14$. Anticipated results for two different parameterizations of ΔG are plotted in Fig. I.1.2-2. Because the observable A_{LL} is quadratic in $\Delta G/G$, the measurement error be-

comes somewhat larger as $\Delta G/G$ becomes small. For example, if the y-axis in Fig. I.1.2-2 were scaled by 0.25, then ~ 10 times the integrated luminosity would be required to achieve the same statistical resolution.

I.1.2.c Asymmetries in Inclusive W^\pm and Z^0 Production

Inclusive W^\pm and Z^0 production at RHIC will be a powerful tool for investigating parton distributions in the proton, and perhaps also in light nuclei. This is due to the large cross section for W^\pm and Z^0 production and to the V-A coupling of the W. With the addition of an electromagnetic calorimeter, the STAR detector is especially well suited for the measurement of inclusive W^\pm and Z^0 production due to its large acceptance for electrons produced by high mass particle decays. The rates for W^\pm and Z^0 decays to electrons within the STAR detector acceptance have been estimated at $\sqrt{s} = 500$ GeV using Pythia to be⁶⁹

$$\begin{aligned}\sigma(pp \rightarrow W^+ + X \rightarrow e^+ + \nu + X) &= 120 \text{ pb} \\ \sigma(pp \rightarrow W^- + X \rightarrow e^- + \nu + X) &= 43 \text{ pb} \\ \sigma(pp \rightarrow Z^0 + X \rightarrow e^+e^- + X) &= 10 \text{ pb} \end{aligned} \quad (\text{I.1.2-12})$$

The W^\pm single spin asymmetries provide a unique and sensitive probe of parton spin dependent distributions. Indeed, the unpolarized \bar{u} and \bar{d} distributions will be well measured at RHIC. Production of W^\pm from polarized protons can determine the polarization of \bar{d} quarks in the proton while corresponding W^- measurements determine the polarization of the \bar{u} quarks. In some models of the proton, the \bar{d} quarks are unpolarized and the \bar{u} quarks are highly polarized⁷⁰.

At $\sqrt{s} = 500$ GeV, from 50,000 to 100,000 W^+ will be produced in a standard run period and about 25% as many W^- . The production of W 's is peaked near central rapidity, with about half of the events produced at rapidity less than 0.5. The observed electron distribution is broader, however, due to the decay distribution of the W.

As an illustration, consider the case of electrons measured in the production of W^- . One can define the incident direction for one of the beams to be positive so that small angle scattering from that beam hits the end-cap. For a d quark in that positive incident beam, W^- production and the parity violating decay will produce an electron at relatively small forward angles. The kinematics and structure functions for d and \bar{u} quarks will tend toward the selection of a d quark with larger x than that of the \bar{u} antiquark and thus positive rapidity for the W^- .

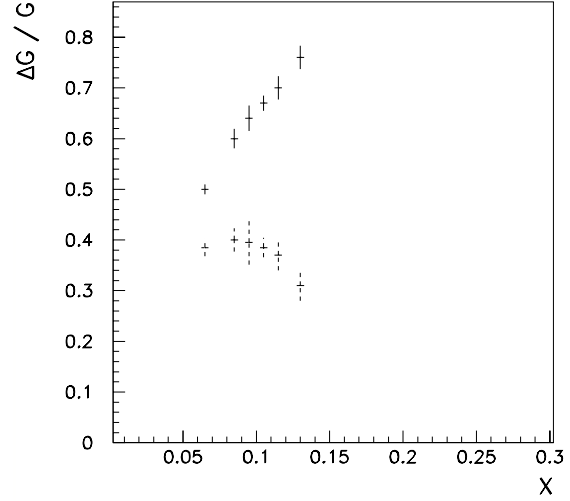


Figure I.1.2-2. Predicted values of $\Delta G/G$ as a function of x for two different parameterizations of ΔG .

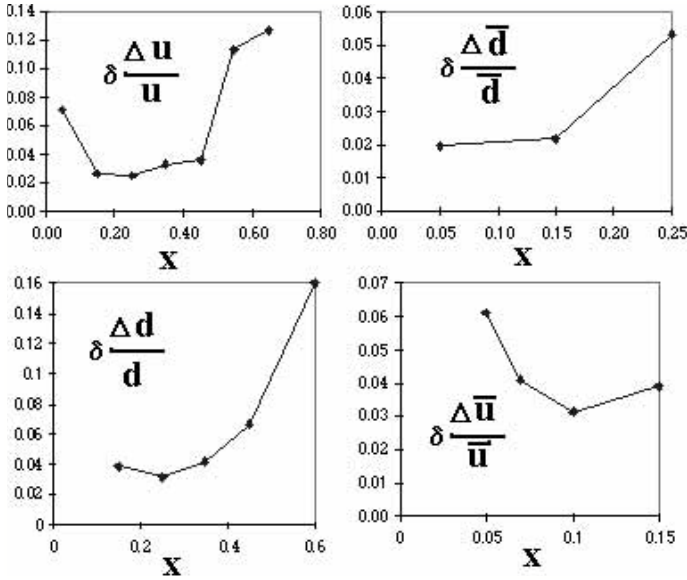
⁶⁹A.A. Derevschikov and V.L. Rykov, Brookhaven National Laboratory report RSC-BNL/IHEP-4 (1992).

⁷⁰C. Bourrely and J. Soffer, Nucl. Phys. B **423**, 329 (1994).

Therefore in the central rapidity region, W^- 's are produced with d quarks from either incident beam, but at larger (positive) rapidity, W^- 's are produced mostly with d quarks from the proton that was moving in the positive direction.

Thus, the electrons observed with $|\eta| > 0.5$ are most interesting because the incident direction of the d quark is more certain. For forward W^- events, we can define a single spin asymmetry A_L by flipping the spin of either beam. With one choice we measure $A_L = \Delta d/d$; with the other choice we measure $A_L = \Delta \bar{u}/\bar{u}$.

Recent results from the SMC collaboration illustrate the difficulty in assigning the x dependence of the quark contribution to the proton spin to specific quark and antiquark flavors⁷¹. In the region of x covered by STAR, the results from the W measurements should reduce the uncertainty in Δu , $\Delta \bar{u}$, Δd , and $\Delta \bar{d}$ by nearly an order of magnitude compared to errors reported by SMC (see Fig. I.1.2-3). The results are for a barrel and one endcap calorimeter.



I.1.2.d High-Energy Drell-Yan Electrons and the Sea Quark Polarization

The study of Drell-Yan pair production appears to be another way to determine the polarization of sea quarks. The $q\bar{q}$ annihilation into a vector boson gives a large asymmetry on a partonic level and selects sea antiquarks along with valence quarks.

The asymmetry A_{LL} for Drell-Yan production in pp collisions is related to the sea quark helicity distribution $\Delta q(x)$,

Figure I.1.2-3. Measurement error for quark and antiquark polarizations vs. x from W decays.

$$A_{LL} = \hat{a}_{LL} \frac{\sum_i e_i^2 [\Delta q_i(x_1) \Delta \bar{q}_i(x_2) + \Delta q_i(x_2) \Delta \bar{q}_i(x_1)]}{\sum_i e_i^2 [q_i(x_1) \bar{q}_i(x_2) + q_i(x_2) \bar{q}_i(x_1)]} \quad (I.1.2-13)$$

where e^2 is the square of the parton charge, and $A_{LL} = -1$. The sum in Equation I.1.2-13 is taken over parton flavor.

To determine if the study of Drell-Yan production might be possible, the PYTHIA event generator was used to estimate the yield in an ideal detector with the same total acceptance as the STAR barrel and endcap calorimeters. The results are presented in Table I.1.2-1 for a standard run at $\sqrt{s} = 200$ GeV.

⁷¹ B. Adeva *et al.*, Phys. Lett B **369**, 98 (1996).

$M_{pp} \text{ (GeV/c}^2\text{)}$	5-9	9-12	12-15	15-20
Events	28,000	20,000	8,400	5,400

Table I.1.2-1. The estimated yield of Drell-Yan pairs in the acceptance of the STAR barrel and endcap calorimeters.

I.1.2.e New Physics

In January 1996 several groups⁷² proposed a new neutral gauge boson Z^0 coupling only to quarks as an explanation of the R_b anomaly at LEP. In May 1996, J. Lopez and D. Nanopoulos proposed a theoretical basis in superstring-derived flipped SU(5) for such a Z^0 ⁷³. The Z^0 in their model is naturally maximally parity violating with only left-handed coupling to u quarks. They concluded following a Marseilles paper⁷⁴ that this effect would be observable at RHIC. Although the interest in the R_b anomaly has waned, the flipped SU(5) Z^0 has no necessary effect on R_b so that Z^0 is still interesting.

We have made a preliminary study of STAR's ability to detect this Z^0 . The observable effect is in the parity violating asymmetry $A_{pv} = (\sigma_{-} - \sigma_{+})/(\sigma_{-} + \sigma_{+})$, where the process measured is inclusive jet production. There is a small A_{pv} (1 to 3% depending on jet E_T) in the standard model arising from t-channel interference between the gluon and the Z in quark-quark elastic scattering. This interference would be increased by a factor of 1.5 to 3 given the presence of a Z^0 from this model, as shown in Fig. I.1.2-4. For this study we chose jets with cone $R=0.5$ which can be measured accurately within $|\eta| < 0.5$. Given an integrated luminosity of 800 pb^{-1} , STAR would see a significant departure from standard model A_{pv} for $m_{Z^0} < 600 \text{ GeV}$.

The standard model A_{pv} will be an interesting measurement in itself since it is a prediction of the standard model that has not previously been experimentally verified. The standard model A_{pv} as measured by STAR with 800 pb^{-1} is shown in Fig. I.1.2-5.

I.1.2.f Transverse Quark Structure Functions of the Proton

There exists a third fundamental partonic structure function $h_1(x)$, which is a leading-twist distribution function like $f_1(x)$ and $g_1(x)$. This distribution can be determined by measuring the transverse spin asymmetry A_{TT} in Z production,

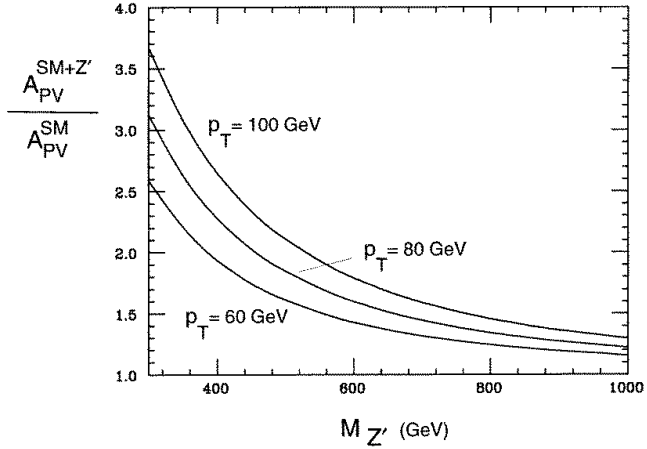


Figure I.1.2-4. Increase in the inclusive jet production parity violating asymmetry A_{pv} for three values of jet p_T .

⁷² P. Chiappetta, J. Layssac, F. Renard, and C. Verzegnassi, hep-ph/9601306; G. Altarelli, N. Di Bartolomeo, F. Feruglio, R. Gatto, and M. Mangano, hep-ph/9601324.

⁷³ J. Lopez and D. Nanopoulos, hep-ph/9605359.

⁷⁴ P. Taxil and J. Virey, hep-ph/9604331.

$$A_{\text{TT}} \equiv \frac{\sigma^{\uparrow\uparrow} - \sigma^{\uparrow\downarrow}}{\sigma^{\uparrow\uparrow} + \sigma^{\uparrow\downarrow}}. \quad (\text{I.1.2-14})$$

$A_{\text{TT}} = \hat{a}_{\text{TT}} \frac{h_1^q}{q} \frac{h_1^{\bar{q}}}{\bar{q}}$ when one flavor is dominant. If $h_1^{\bar{q}}$ is close to zero, we can not measure

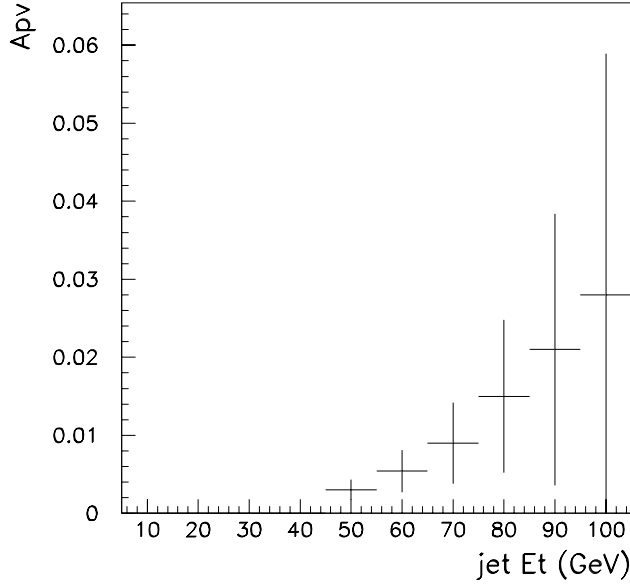


Figure I.1.2-5. Predictions of the standard model for the parity violating asymmetry A_{pV} .

The event rate for direct- γ production can be estimated for the EMC barrel as in Section I.1.2.b. The corresponding estimate for the uncertainty in the single transverse spin asymmetry is

$$\delta A_T \approx \pm 0.006 \sqrt{\frac{320 \text{ pb}^{-1}}{\int \ell dt}}. \quad (\text{I.1.2-15})$$

I.1.3 Trigger Concept and Capability

A sensitive trigger is essential for STAR. Rare phenomena can be studied effectively only if a selective trigger is employed. The STAR EMC provides a large range of possibilities for triggering in AA, pA, and pp collisions at RHIC.

I.1.3.a Event Selection in AA Collisions

The most interesting collisions at RHIC are those that produce the highest densities and temperatures. These collisions are the most promising environment in which to search for novel phenomena and signatures of a deconfined phase of quarks and gluons. A characteristic feature of these conditions is the observation at mid-rapidity of high particle multiplicities and high transverse energy deposition. If the mean p_t per particle and

h_1 . However, we can measure $h_1(x)$ in dijet production from $A_{\text{TT}} = \hat{a}_{\text{TT}} \left(\frac{h_1^q}{q} \right)^2$ at high p_t where quark-quark scattering dominates. These measurements are unique to the STAR detector.

I.1.2.g Higher Twist Effects

Single transverse spin asymmetries are expected to vanish in lowest order, perturbative QCD. Even though the asymmetries vanish at the leading, or “twist-2” level, this is no longer true when higher order, “twist-3” diagrams are taken into account. For example, a large single spin asymmetry has been predicted in inclusive direct- γ production ($p^\uparrow p \rightarrow \gamma + X$).⁷⁵

⁷⁵J. Qiu and G. Sterman, Phys. Rev. Lett. **67** (1991) 2264.

the global ratio of neutral to charged particle energy do not vary significantly from event to event, central impact parameter triggers based on the multiplicity of charged particles or the total transverse energy are essentially the same. However, exciting phenomena that can occur in central AA collisions such as disordered chiral condensates (CC) or Bose-Einstein condensates (BE) may alter the relationship between charged particle multiplicity and transverse energy. The STAR Central Trigger Barrel (CTB) is sensitive to the multiplicity of charged particles (mainly charged pions) while the EMC is sensitive to energy emitted in the form of electrons and photons (mainly photons from the decay of neutral pions). Thus the combination of the EMC and the CTB can provide information about the relative numbers of charged pions and neutral pions.

I.1.3.b Use of EMC for Selection of Rare Events in AA Interactions

It is in the selection of rare events in AA interactions that some of the unique capabilities provided by the electromagnetic calorimeter become apparent. As noted above, some of the most interesting physics may be found by triggering on events in which the average p_t per particle^{76,77} and/or the ratio of charged to neutral energy^{78,79} depart significantly from that which is characteristically observed. If these events occur at low cross section and their observation therefore requires significant rejection of “background events” at the trigger level, they will not be observed unless the characteristic correlation between the charged-particle multiplicity and transverse energy can be tested at the trigger level. In the present circumstance in which full event reconstruction (i.e., tracking) will take longer than 10 ms, this correlation can not be accomplished for events having an unusual $\langle p_t \rangle$ without the electromagnetic calorimeter. Of course, searching for events exhibiting an unusual charged-to-neutral energy ratio cannot be accomplished in any circumstance without measurement of the neutral electromagnetic energy. With partial coverage of the electromagnetic calorimeter it would still be possible to search for rare events in selected regions of the STAR acceptance, although the sensitivity would be reduced.

To test the sensitivity of the STAR EMC to events exhibiting unusual isospin abundances, the response of this detector was examined in a full GEANT simulation of the STAR detector, using 75 “normal” central AuAu events generated using HIJING at $\sqrt{s_{nn}} = 200$ GeV/nucleon. The same events with 50% of the π^\pm mesons changed to π^0 mesons are used to estimate the response of STAR to phenomena like disordered chiral condensates (CC). To simulate the response of STAR to phenomena like Bose-Einstein condensates (BE), the momentum of the pions from the normal events were lowered by 30% and 30% more particle were added to conserve energy.

The results of these simulations are shown in Fig. I.13-1, in which the total sampled energy deposited in the EMC barrel has been plotted versus the charged particle multiplicity detected in the central trigger barrel for both the normal and anomalous AuAu collisions. The open circles represent HIJING calculations for the full range of

⁷⁶L. Van Hove, Phys. Lett. 118B, (1982) 138.

⁷⁷M. Kataja *et al.*, Phys. Rev. D34, (1986) 2755.

⁷⁸J.D. Bjorken, Acta Physica Polonica B23, (1992) 635.

⁷⁹F. Wilczek, {Chiral Dynamics Near Equilibrium or After Quenching,” Proceedings of the Tenth International Conference on Ultra-Relativistic Nucleus-Nucleus Collisions, June 20–24, 1993, Borlänge, Sweden.

impact parameter possible in AuAu reactions. The closed circles represent normal HIJING calculations for $0 \text{ fm} < b < 2.5 \text{ fm}$. The open triangles stand for the BE events while the open squares signify the CC events. The minimum bias HIJING events fall on a straight line that passes through zero which implies that the ratio of EMC energy to CTB multiplicity is constant for normal events. The anomalous events also fall on a line that passes through zero but with a different slope.

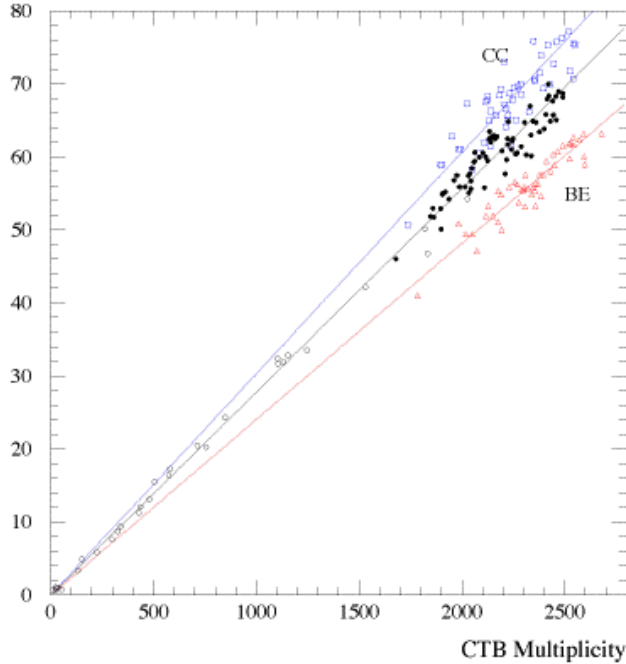


Figure I.1.3-1. HIJING calculations for AuAu collisions filtered through GEANT for STAR. The open circles represent normal HIJING calculations over all impact parameters. The closed circles depict central HIJING events with $b \leq 2.5 \text{ fm}$. The open triangles show the same events with the momentum of the pions reduced by 30% and the multiplicity increased by 30% while the open squares represent the same events with 50% of the charged pions changed to neutral pions.

These distributions are obtained by fitting a Gaussian to the results for the full GEANT simulations and producing new distributions with the same centroids and widths. These distributions represent 10^8 AuAu events, which would represent 100 days of RHIC running at 1 event per second. However, these distributions could be acquired much more quickly if only the EMC and CTB were recorded. Assuming 1000 events per second EMC/CTB-only events, these distributions could be obtained in 1 day and could be used to set trigger levels on rare events.

The ratio of the energy deposited in the EMC barrel to the charged particle multiplicity detected in the CTB has been histogrammed in Fig. I.1.3-2 for the same events. In the left panel, the histograms are shown for the full barrel. The two kinds of anomalous events are clearly separated from the normal events. In the right panel, the same events are observed with a full GEANT calculation incorporating 1/4 of the barrel. Although the sensitivity is decreased somewhat, it is still possible to trigger on isospin fluctuations.

To gain an understanding of the EMC trigger with respect to isospin fluctuations, one can investigate the response to different fractions of charged pions being changed to neutral pions. In Fig. I.1.3-3, the distributions of the ratio of the EMC to the CTB for ordinary HIJING events (solid line labeled xx) and for CC events assuming 20% (dotted line), 40% (dashed line) and 50% (solid line labeled cc 50%) of the charged pions change to neutral pions are given.

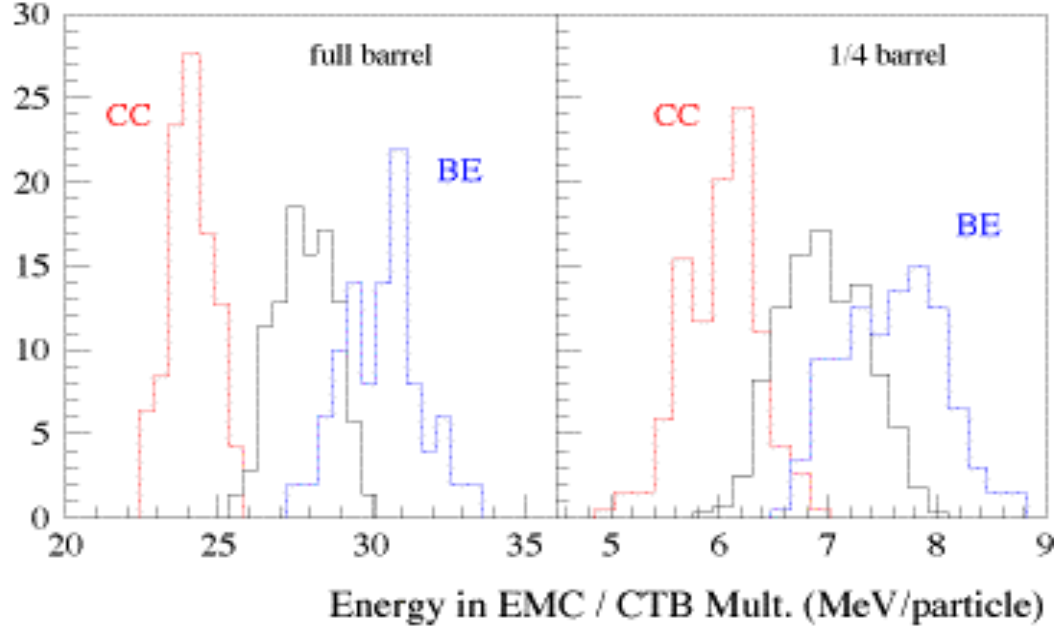


Figure I.1.3-2. Histograms of the energy in the EMC divided by the charged particle multiplicity in the CTB for the events shown in Figure I.1.3-1. The solid lines depict normal HIJING events while the dashed lines show the chiral condensate (CC) events and the dot-dashed lines represent the Bose-Einstein (BE) events. The left panel shows simulations for the full barrel while the right panel shows the same events measured with 1/4 of the barrel calorimeter.

In Fig. I.1.3-3b, similar results are shown for the case where one assumes that the CC effects only occur for low p_t pions. The ordinary HIJING events and the 50% CC events are the same as in Figure I.1.3-3a. The dotted (dashed) line represents events in which all the charged pions with momenta below 300 (500) MeV/c change to neutral pions which is 34 (63) % of all the emitted pions. Thus one can see that a trigger based on the EMC can be sensitive to various types of anomalous isospin fluctuations.

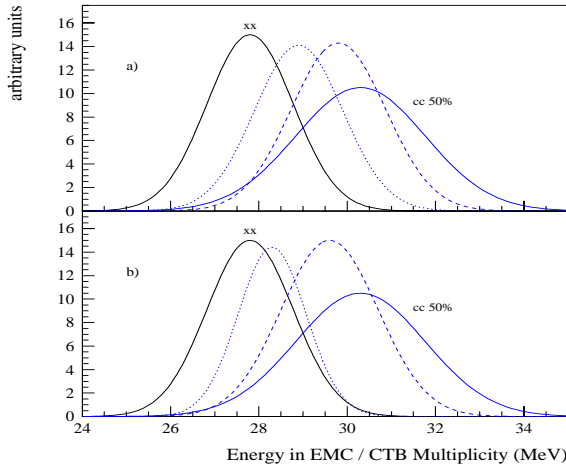


Figure I.1.3-3. Distributions extracted by fitting fully analyzed HIJING events for AuAu collisions using different assumptions about chiral condensates. These curves all have the same number of events. See text for explanation.

To trigger on rare events, one must be able to select a few interesting events from a large background of uninteresting events. To estimate the ability of the EMC we have constructed several sets of events in which the relative probability of occurrence is varied as well as the fraction of charged pions converted to neutral pions. In Fig. I.1.3-4a, the relative probability of occurrence is varied along with the fraction of charged pions converted to neutral pions. The solid line marked cc depicts the normal AuAu events. The solid line labeled cc 50% shows the case in which

one assumes that chiral condensates with 50% of the charged pions changing to neutral pions occur with 0.1% of the probability of normal events. The dashed curve represents the case where 40% of the charged pions change and these events occur with 1% of the normal probability. The dotted curve stands for events in which 20% of the charged pions flip with 10% the normal probability.

Within the assumptions of the schematic calculations, one can see that it would be possible to set a trigger level on the ratio EMC/CTB to select isospin fluctuations.

In Fig. I.1.3-4b, the effect of only lower momentum charged pions changing sign is shown. The solid lines labeled xx and cc 50% are the same as in Fig. I.1.3-4a. The dotted line shows the effect of all the charged pions with momenta below 300 MeV/c (34% of the total number of pions) changing to neutral pions with 10% the probability of normal events. The dashed line shows the distribution of ratios for the case of all the charged pions with momenta below 500 MeV/c (63% of all pions) occurring with 1% the frequency of normal events.

One can see from Fig. I.1.3-4b that separating events where charged pions with momenta less than 300 MeV/c from normal events would be impossible. However, in the case of charged pions with momenta below 500 MeV/c, flipping could be selected.

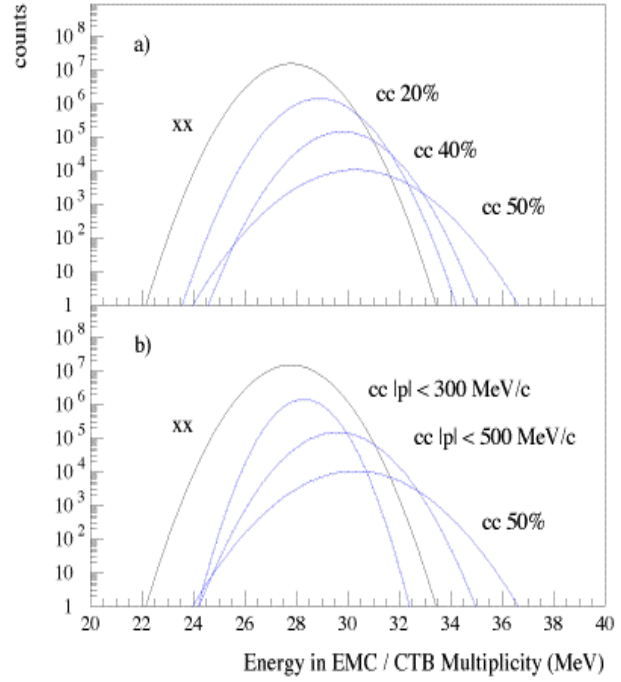


Figure I.1.3-4. Distributions extracted by fitting fully analyzed HIJING events for AuAu collisions using different assumptions about the occurrence of chiral condensates. See text for explanation.

I.1.3c Triggering on Jets and Photons in pp and pA

The study of hard parton scattering in pp and pA reactions in the form of jets and hard photons is crucial to the interpretation of AuAu results. In addition, the measurements of jets and hard photons are fundamental to the spin physics program using polarized pp reactions. The EMC provides a sensitive and selective trigger for these phenomena. In Fig. I.1.3-5, the sensitivity of the EMC to triggering on 20 GeV jets and photons is shown using fully reconstructed HIJING events for pAu reactions at $\sqrt{s} = 200$ GeV for two cases. In the left panel, a correlation is made between the total energy observed in the EMC versus the maximum energy observed in the $(\Delta\eta, \Delta\phi) = (0.05, 0.05)$ highest trigger towers for events without jets, events with 20 GeV jets, and events with 20 GeV photons. In the right panel, the same events are studied with an overlapping patch size of $(\Delta\eta, \Delta\phi) = (0.8, 0.8)$. For the case of $(0.05, 0.05)$, the photons are clearly separated from the jets while the jets have some overlap with the nojet events. For the $(0.8, 0.8)$ patches, the trigger separates the jets more cleanly from the nojet events while overlapping slightly more with the photons, which are not affected by the different patch sizes.

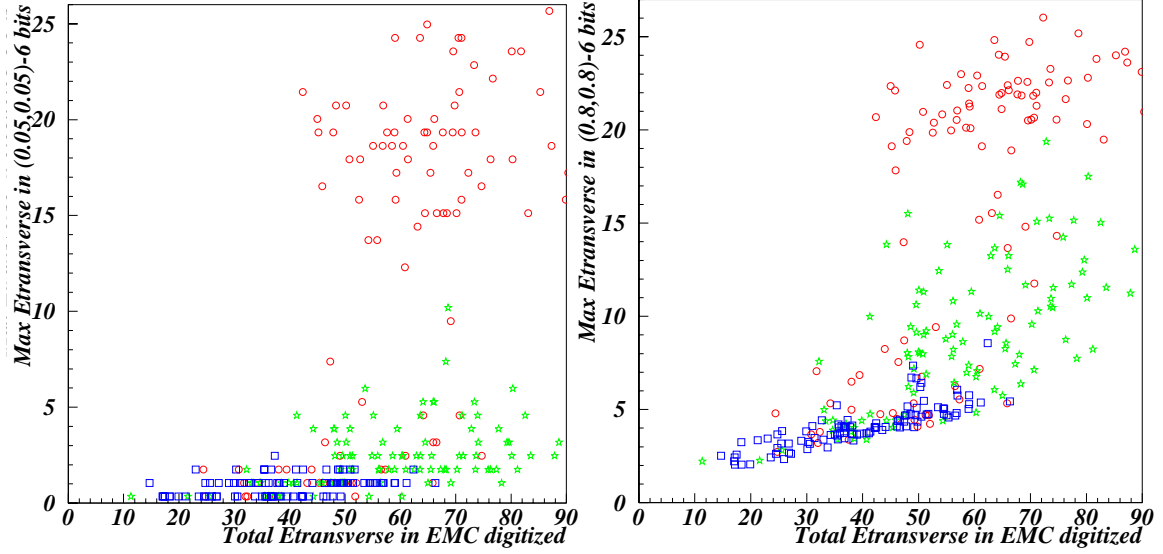


Figure I.1.3-5. Results for HIJING pp events filtered through the STAR analysis software for the (0.05,0.05) high towers (left) and the (0.8,0.8) patches (right).

The proposed lowest level trigger system hardware involves 300 $(\Delta\eta, \Delta\phi) = (0.2, 0.2)$ trigger towers in the calorimeter. Each trigger tower is digitized to an accuracy of 6 bits. In addition, the highest tower within each trigger tower (0.05,0.05) will also be digitized to 6 bits. Higher levels of the trigger system can then produce overlapping patches of (0.8,0.8) from these trigger towers. To model the response of the trigger to jets and photons, using these assumptions, we have compared the number of events with 20 GeV jets above a given threshold on the (0.05,0.05) high towers to the number of 20 GeV photons above the same threshold using HIJING calculations for $\sqrt{s} = 200$ GeV pAu filtered through the STAR acceptance. These results are presented in Fig. I.1.3-6.

To illustrate the effect of digitization, the results for the (0.05,0.05) trigger patches are compared with similar results using (0.8,0.8) patches calculated using the STAR trigger electronics and processors assuming a full-scale value of 40 GeV digitized to 6 bits. These results are shown in Figure I.1.3-7.

There is little difference between the full accuracy signals and the 6 bit signals for the (0.05,0.05) patches while an effect is observed jets in the (0.8,0.8) patches. One effect of the digitization for the (0.8,0.8) patches is simply a shift in the sum due to the finite width of the bins.

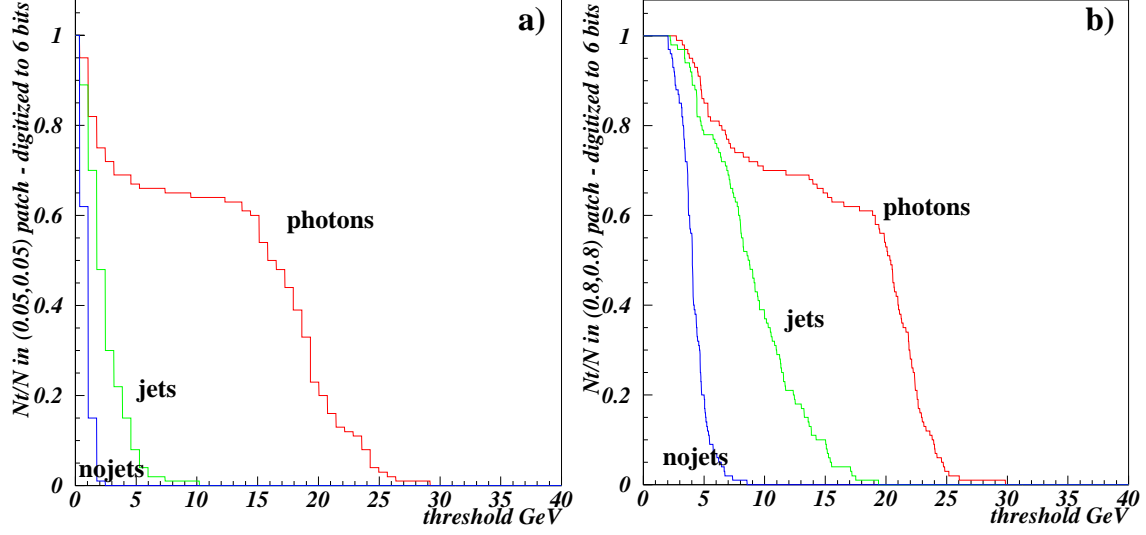


Figure I.1.3-6. Trigger efficiency for 20 GeV jets and photons and no jet events for the thresholds on the high tower bits (0.05,0.05) and (0.8,0.8) overlapping patches.

With these results for jets and direct photons at 20 GeV and other energies along with the known cross sections for the production of jets and photons, one can predict the counting rate for the design luminosity of $1 \times 10^{32} \text{ s}^{-1} \text{ cm}^{-2}$. In Fig. I.1.3-8, the counting rates for jets and photons from $\sqrt{s} = 200 \text{ GeV}$ pAu interactions are shown as a function of the threshold on (0.05,0.05) high towers and (0.8,0.8) patches in the EMC.

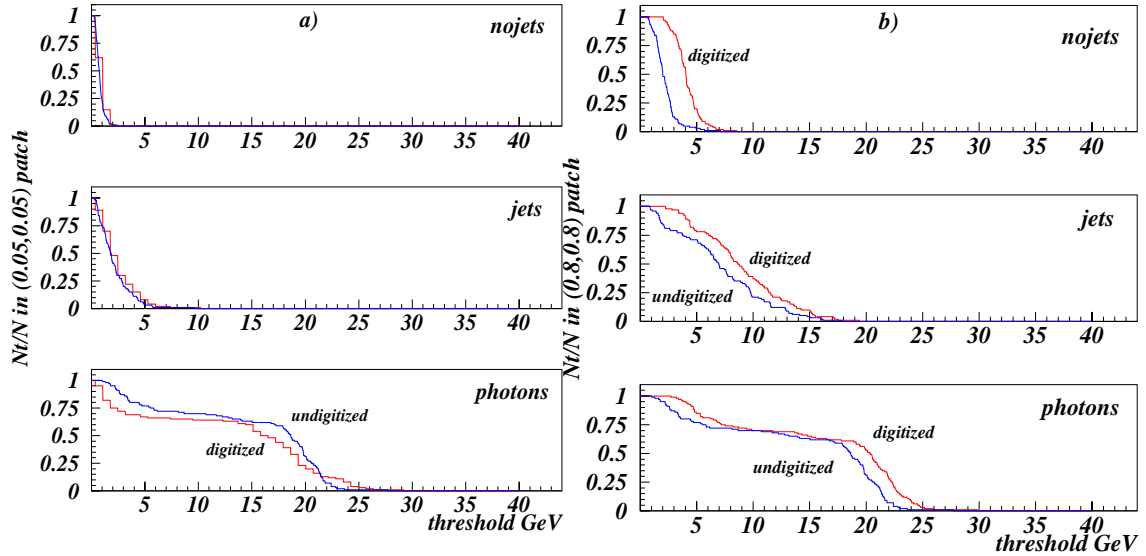


Figure I.1.3-7. Effect of digitization on the trigger efficiency for nojets, 20 GeV jets, and 20 GeV direct photons from pAu interactions.

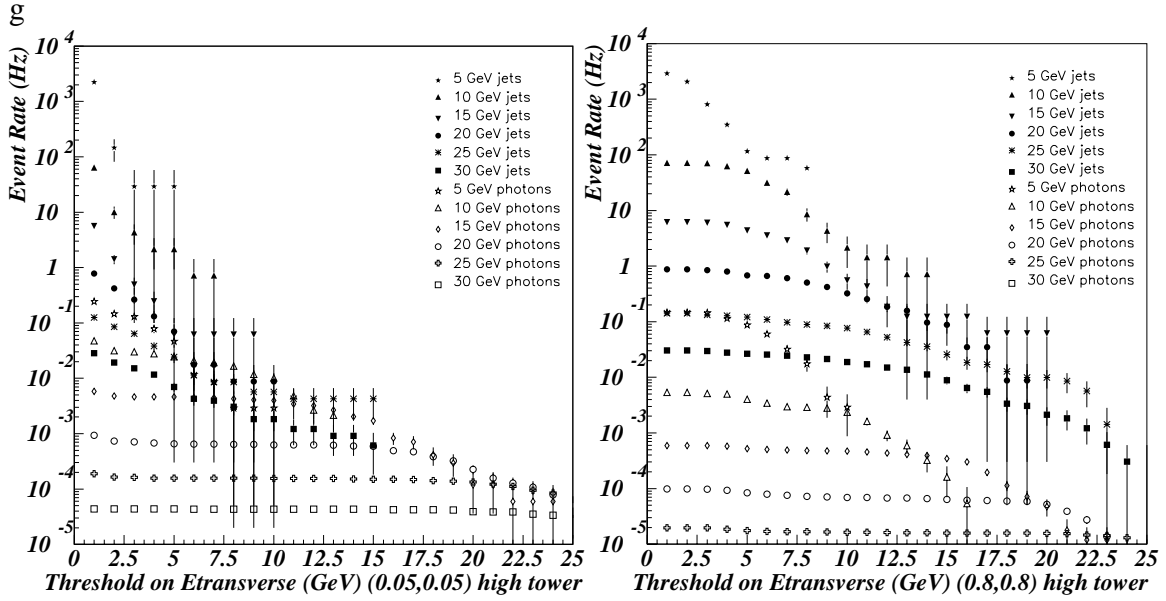


Figure I.1.3-8. Predicted counting rates for pAu reactions based on threshold on the (0.05,0.05) high towers and the (0.8,0.8) patches for various energy jets and direct photons using the design luminosity, extracted efficiencies, and calculated jet and direct photon cross sections.⁸⁰

I.2 Detector Concept

I.2.1 Choice of Technology

A priori, there are many available technologies for an electromagnetic calorimeter. Crystals such as NaI, CsI and BGO have excellent resolution for individual low energy photons. Lead glass has better energy resolution than most sampling calorimeters. The primary problem with these detectors is cost, particularly for the depth, area, and geometry needed for STAR. The area that must be covered outside the TPC is over 100m^2 for $|\eta| < 2$. To accomplish all the physics goals, the depth must be adequate to contain 40GeV showers within a few percent, including leakage fluctuations. This requirement implies a total depth of approximately $20X_0$. The geometrical constraint imposed by the solenoidal STAR geometry implies the EMC elements must be wedge-shaped at a minimum, if not truncated pyramid shapes as used in VENUS and UA2.

Gas calorimetry with wire chamber sampling between layers of lead has been used in some applications, but in general has demonstrated problems with non-uniform gain and extremely large signals from neutrons. Other sampling detectors have used liquid argon or some other liquid to detect the ionization caused between plates of converter or absorber by the passage of charged particles. Generally, the cryogenic vessels used to contain the liquid take up an unacceptable amount of space. This geometry leads to a lack of hermiticity and cracks within the sensitive volume of the detector. Liquid argon

⁸⁰ W. Christie and Hard Processes in Hadronic Interactions, Int. J. Mod. Phys., A10, 2881, LBL-36948 (CERN-95-05).

calorimeters also typically require more time to integrate signal than for example, scintillator tiles, although there was progress on this aspect with an SSC liquid krypton prototype. Although detailed studies of a liquid argon calorimeter were not performed, both the cost and GeV equivalent noise level are expected to be higher than for a lead-scintillator sampling calorimeter. The noise level can be a particularly serious problem in the present application, because for heavy ion interactions, the average p_t of the charged particles and photons that reach the calorimeter is less than 400 MeV/c.

A sampling calorimeter using lead and plastic scintillators has been chosen for the detection of electromagnetic energy in STAR. A significant advantage of this technology is that the calorimeter can be constructed from a number of relatively small modules. This approach will permit part of the calorimeter to be constructed and installed after the STAR baseline components (TPC, magnet, etc.) are complete. This staging would be significantly more difficult, for example, with liquid argon technology. Calorimeters of this design have been successful in a number of colliding beam and fixed target experiments, and as a consequence, the technology is well known. Recent examples of detectors incorporating this technology include the endcap upgrade for CDF and the proposed barrel calorimeter for SDC. In particular, the use of a lead-scintillating sampling calorimeter is a cost-effective way to cover the necessary area, employing a mechanical design flexible enough to accommodate the constraints imposed by the closed STAR geometry. The energy resolution is adequate to reconstruct π^0 's of p_t well below 2 GeV/c. For some kinds of measurements in heavy ion physics where a large number of very low energy photons are to be summed, the resolution is also adequate. The intrinsic resolution expected from sampling calorimeters with 5 mm ($\sim 0.9 X_0$) lead plates is $\sim 14\% / \sqrt{E}$. With typical photostatistics (two photoelectrons / sampling layer / minimum ionizing particle) the resolution typically achieved is $16\% / \sqrt{E}$ plus a 1%-3% constant term (confirmed in STAR test beam runs and simulations). The constant or so-called "stochastic" term comes from tower-to-tower variations in the calibration and transverse and longitudinal non-uniformities in light collection from the pieces of scintillator.

The light generated by charged particles passing through the scintillator must be brought to photon detectors such as photomultipliers. In the STAR design the electromagnetic calorimeter will be located inside the solenoidal magnet. The photomultipliers must be located outside the magnet to avoid high magnetic fields, and to minimize the radius and cost of the magnet. The use of waveshifter plates such as those used in the CDF and ZEUS calorimeters would not be practical, because they would take up an unacceptable amount of space in traversing the coil pancakes. Consequently, plastic optical fibers that take up less space and require less labor to prepare have been selected for the STAR design.

Once the decision is made to use a sampling calorimeter with scintillator, the next concerns are how best to accomplish efficient light collection, what segmentation should be used, and how the mechanical structure should be designed. These choices are related and are discussed in detail in the sections that follow.

In order to make a choice of the technology for the shower maximum detector (SMD), three different SMD prototypes were tested inside a small EMC prototype at the BNL test beam over a period of two years. The scintillator strip version similar to the one used in the CDF endplug upgrade functioned well, but would have been very difficult to fit into the space available in STAR. The cost of over 3×10^4 phototube channels,

even with multi-anode tubes, was also a serious consideration. We have decided on the wire-strip gas detector. In beam tests of our design showed that our detector performed extremely well and as expected on the basis of CDF experience.

I.2.2 Summary of the Mechanical Structure

The barrel Electromagnetic Calorimeter, EMC, is located inside the aluminum coil of the STAR solenoid and covers $|\eta| \leq 1.0$ and 2π in azimuth, thus matching the acceptance for full TPC tracking and is shown schematically in Fig. I.2.2-1

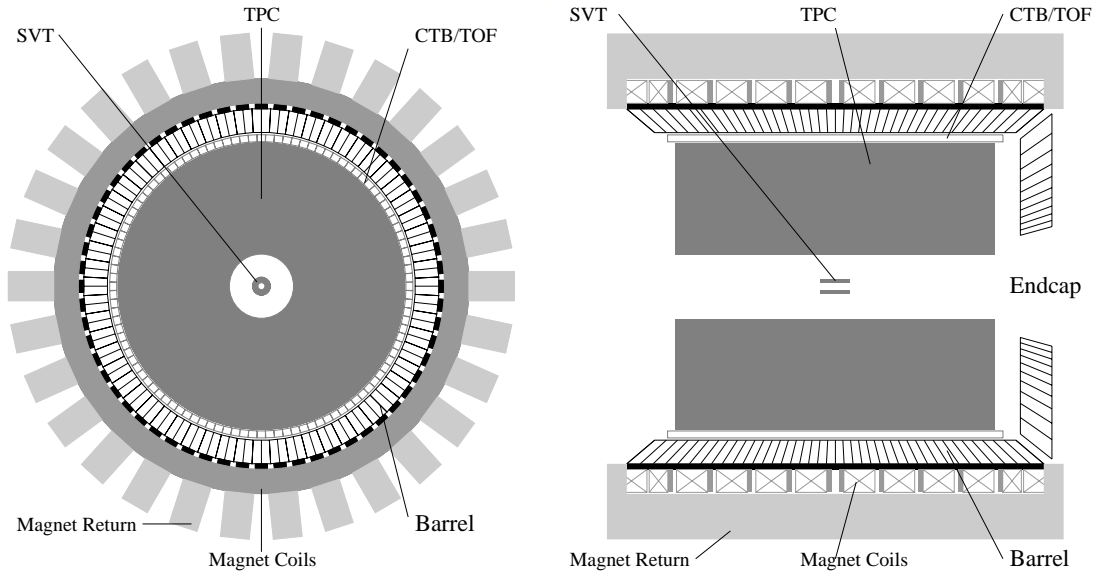


Figure I.2.2-1. Cross sectional views of the STAR detector. The barrel EMC covers $|\eta| \leq 1.00$. The Endcap Calorimeter covers $1.05 \leq \eta \leq 2.0$. The barrel EMC modules slide in from the ends on rails which are held by aluminum hangers which attach to the magnet iron between the magnet coils. Optical fibers from the towers pass through spaces between the coils and are subsequently routed between the iron flux return bars to the exterior of the magnet.

The design for the barrel electromagnetic calorimeter includes a total of 120 calorimeter modules, each subtending 6° in ϕ (0.1 radian) and 1.0 unit in η . These modules are mounted 60 in ϕ by 2 in η as shown in Fig I.2.2-1. Each module is roughly 26cm wide by 293cm long with an active depth of 23.5cm plus about 6.6 cm in structural plates. A module is further segmented into 40 towers, 2 in ϕ and 20 in η , with each tower being 0.05 in $\Delta\phi$ by 0.05 in $\Delta\eta$. The calorimeter is thus physically segmented into a total of 4800 towers, each of which is projective and pointing back to the interaction diamond. Figure I.2.2-2 shows a side view of a module illustrating the projective nature of the towers in the η -direction.

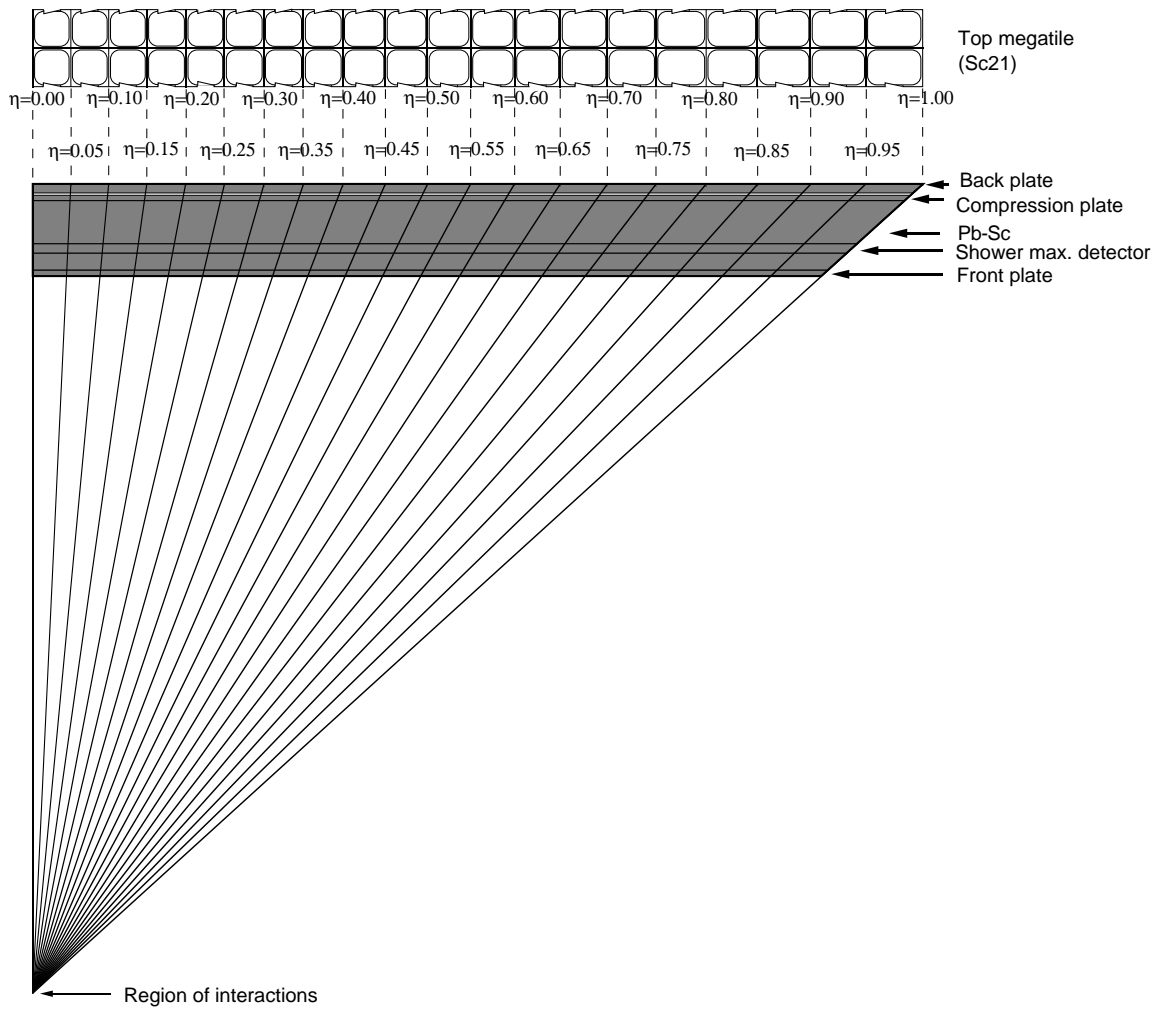


Figure II.2.2-2. Side view of a calorimeter module showing the projective nature of the towers. The 21st megatiles layer is also shown.

The STAR EMC is a sampling calorimeter, and the core of the structure consists of a lead-scintillator stack and a shower maximum detector situated approximately 5 radiation lengths from the front of the stack. There are 20 layers of 5mm thick lead and 21 layers of 5mm thick scintillator. This core structure, the stack, is held together by friction aided by compressional forces. The compression is applied by a combination of 30 straps connecting the non-magnetic front and back plates of the structure, and a system of bolts and spring-loaded washers between the back plate and a compression plate. The plastic scintillator is in the form of “megatiles”, with 40 optically isolated “tiles” or segments in each layer as shown in figure II.2.2-2.

I.2.3 Summary of the Optical Structure

The Solenoidal Tracker detector of RHIC employs scintillating tile/wavelength shifting fiber readout technology⁸¹ for the Barrel Electromagnetic Calorimeter. A significant advantage of this technique is that the calorimeter dead space can be made small compared to calorimeters based on the conventional scintillating plate / wavelength shifting bar read-out scheme. This technique has been successful in number of colliding beam and fixed target experiments, and as a consequence, the technology is well known. Recent examples of detectors incorporating this technology include the endcap upgrade calorimeter for CDF⁸².

The design of the Barrel EMC comprises 120 calorimeter modules, each subtending 6° in ϕ (0.1 radian) and 1 unit in η where ϕ is the azimuthal angle in radians and η is the pseudorapidity. The calorimeter is a sampling calorimeter and the core of the structure consists of a lead-scintillator plate stack. There are 21 active scintillator layers of 5-mm thick alternating with 20 layers of 5-mm thick lead absorber plates. This core structure, the stack, is held together by friction and is compressed to 15 PSI to increase the frictional forces. The plastic scintillator is in the form of “mega-tiles” with 40 optically isolated “tiles” or segments in each layer. In order to simplify handling, the mega-tiles are produced from two pieces of approximately 1.6 m long scintillating plates for each layer in the calorimeter. The signal from each scintillating tile is read-out with a single wavelength shifting (WLS) fiber embedded in a σ -groove that is machined in the tile. After exiting the scintillator, the WLS fiber is routed along the side of the stack and terminated at a multi-fiber, optical connector at a back-plate of module. From there, 3.5 m long, multi-fiber, optical cables of clear fibers carry the light from optical connector through the magnet structure to decoder boxes containing the photomultiplier tubes (PMT's), where the light from tiles comprising a single tower are merged. A light mixer is placed between these fibers and the photocathode of PMT to optimize the uniformity of the distribution of light across the photocathode. A schematic diagram of tile/fiber optical read-out scheme of Barrel EMC is shown in Figure I.2.3-1

We use extruded, polystyrene-based, scintillator (PS) as the active medium of calorimeter. For the WLS fiber, we use Kuraray multiclاد Y11 (200 ppm) S-type wavelength shifting fiber, 0.83 mm in diameter. One end of the wavelength shifting fiber will be polished and aluminum sputtered. The clear fibers will be Kuraray double-clad fiber 0.9 mm and 1.0 mm in diameter. As a photodetector we will use green extended photomultiplier FEU115-M. The non-polished mega-tile edges are painted white with Bicorn BC620 reflective paint. White bond paper, which has a high coefficient of friction, is used on both sides of the mega-tile as a reflector. With typical photostatistics (two photo electrons/sampling layer/minimum ionizing particle) and typical sampling frequency (once every $0.9X_0$), the intrinsic resolution expected from such a sampling calorimeter is about $16\%/\sqrt{E}$ plus a 1.5% constant term added in quadrature. The constant or so-called

⁸¹ V.I.Kryshkin and A.I.Ronzhin, Nucl.Inst. and Meth. A247(1986)583. M.G.Albrow et al., Nucl. Inst. and Meth. A 256(1987)23.

⁸² G.W.Foster, J.Freeman and R.Hangstrom, Nucl.Phys.B,A23(1991) 93 P.de Barbaro et al., Nucl.Inst.Meth.,A315(1992) 317

“stochastic” term comes from tower-to-tower variations in the calibration and both transverse and longitudinal non-uniformities in light collection from the pieces of scintillator. Based on EMC module in-beam test results⁸³ and simulations, this energy resolution will be achieved in practice with:

- ◆ a light yield from scintillating tile more than 2 p.e./tile/MIP;
- ◆ a surface uniformity of the scintillating tile better than 5% RMS;
- ◆ longitudinal uniformity to a level of less than 10% RMS within each tower;
- ◆ total cross-talk better than 2% between tiles for each of the tiles in the calorimeter.

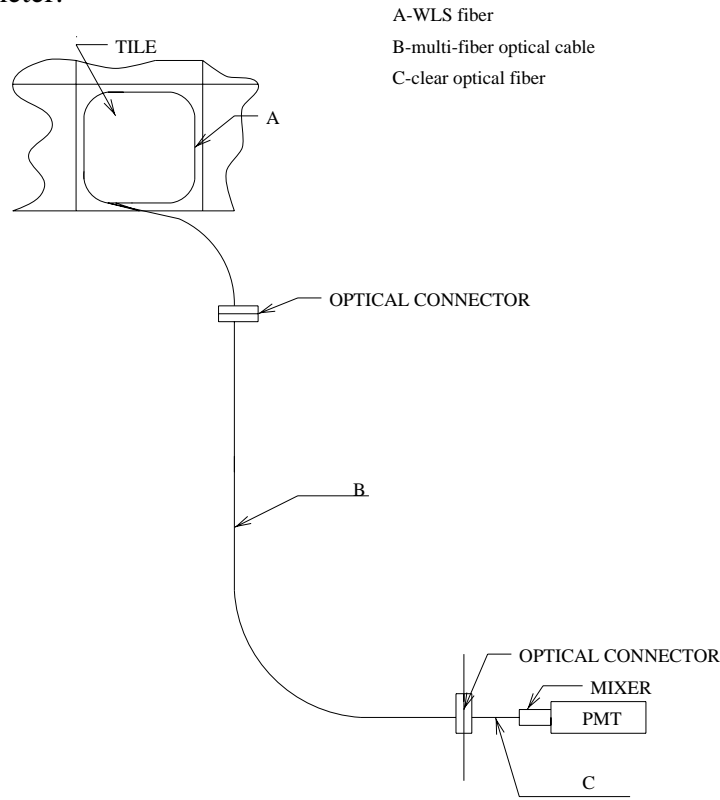


Figure I.2.3-1 A diagram of tile/fiber optical read-out scheme of Barrel EMC.

Much of the technology employed in the STAR EMC optical design has its origins in the original research and development conducted by the SDC, CDF, PHENIX, CMS and ATLAS groups, including megatiles production, preparation of optical components (optical fibers, optical connectors) and fundamental measurements of the tile/fiber optical

⁸³ S.Bennett et al., The EMC and SMD Performance In 1997 Testbeam Run At BNL, STAR NOTE SN.....(To be published)

system. However to achieve optimization of the optical system for STAR, such as the design of tile, scintillating plastic material selection, optical fiber selection and optical connector selection, we have conducted an extensive R&D program described in chapter II.

I. 2. 4 Summary of the Electronics System

The EMC electronics includes trigger, readout of phototube and wire detectors, high voltage system for phototubes, low voltage power, slow controls functions, calibration controls, and interfaces to the STAR trigger, DAQ and slow controls. The bulk of the Front end electronics including signal processing, digitization, buffering, formation of trigger primitives, and the first level of readout is located in custom EMC crates on the outside of the magnet iron. The exception is the preamplifiers and switched capacitor arrays for the SMD wire chambers. They reside on the EMC modules inside the STAR magnet. The EMC part of level 0 trigger is on the Electronics platform in the interaction hall, as is the overall STAR level 0 trigger. The EMC tower data collector is also on the platform. Data and trigger signals follow separate paths from the EMC barrel crates to the platform. The data is then shipped by fiber optics to the DAQ system interface in the counting house.

In STAR, the Level 0 trigger is the only level which does not incur large dead times from the opening of the gated grid in the TPC. The grid cycling rate is limited, and furthermore, there is not a great deal that can be done in the Level 1 system during the TPC drift time of 50 to 100 μ sec. This makes it very important to concentrate as much functionality as possible in Level 0. The EMC is the premier detector for Level 0 because it is fast and it is the only detector sensitive to energy. For reasons of speed and limited bandwidth, the EMC trigger uses trigger primitives instead of the full EMC data. There are two kinds of trigger primitives from the EMC front end. The first set of primitives is the 300 tower sums of 6 bits each from patches of 0.2 by 0.2 in η - ϕ . The second is the 300 high tower values of 6 bits from the single largest 0.05 x 0.05 tower within the 0.2 x 0.2 patch. These primitives are processed in EMC trigger on the platform to make final trigger decision on total E_t , jet triggers, photon triggers, etc. These results are then passed to STAR Level 0 in 700 ns for the final Level 0 decision.

The full resolution data is processed via a separate path from trigger information. The Phototube signals from the towers are integrated and digitized in the front-end cards on every RHIC crossing. These data are pipelined until Level 0 trigger time, and if a trigger occurs it is transferred to a token-addressable memory on the card to await readout. All of STAR utilizes token-addressable memory in order to make a deadtimeless system. The SMD is two layers of wire chamber with pad readout. The signals from the pads are amplified and analog pipelined in a switched capacitor array on the detector before going to the front end processing cards outside the detector.

The EMC data collector on the platform receives signals from each of the crates. This data already has crate number, token number, and a simplified RHIC crossing number included by a multiplexer card in the crate. The collector can do pedestal subtraction, and zero suppression with addition of channel addresses. A standard STAR header for use in event building is also added.

I.2.5 Summary of the Trigger Concept and Functionality

The STAR EMC is designed to provide triggers based on E_t , jets, and direct photons. The STAR Barrel calorimeter consists of 120 modules each covering $0 < \eta < 1$ and $\Delta\phi = 0.1$. Each module has 40 physical towers covering $(\Delta\eta, \Delta\phi) = (0.05, 0.05)$. The basic units of the EMC trigger at lowest level are a sum of 16 physical towers, which produces 300 trigger towers each covering $(0.2, 0.2)$ and the highest physical tower $(0.05, 0.05)$ in each of these trigger towers. These signals are digitized to 6 bits.

The sum of the 300 trigger towers produces E_t , which is used to trigger in AuAu collisions. E_t carries information about the number of π^0 's produced in the reaction. Phenomena that can be selected using the charged particle multiplicity from the central trigger barrel (CTB) and E_t include disoriented chiral condensates and Bose-Einstein condensates that signal the formation of a quark gluon plasma. In addition, trigger patches with $(\Delta\eta, \Delta\phi) = (1.0, 0.8)$ can be correlated with similar patches in the CTB to provide triggering on localized domains of isospin fluctuations.

The high tower information is used to trigger on direct photons and electrons while suppressing jets in pp and pAu reactions. To trigger on jets in pp and pAu reactions, non-overlapping patches of 0.2×0.2 and 1.0×0.8 are used at level 0 and overlapping sums of the trigger towers can be used (subject to level 2 upgrade) to calculate patches with $(\Delta\eta, \Delta\phi) = (0.8, 0.8)$ at level 2.

Thus the STAR EMC will produce the following information for the STAR level-0 trigger:

- 300 trigger towers
($\Delta\eta, \Delta\phi) = (0.2, 0.2)$
6 bits each
- 300 high towers
($\Delta\eta, \Delta\phi) = (0.05, 0.05)$
6 bits each

Given this input, The STAR EMC level 0 trigger output is then

- Barrel $E_t > 3$ threshold; 3 bits (1 bit/threshold)
- Jet tower $(0.2, 0.2) > 3$ thresholds; 3x2 bits (2 bit counters)
- High tower > 3 thresholds; 3x2 bits (2 bit counters)
- Correlation of high tower $>$ threshold and trigger tower $>$ threshold; 2 bits (2 bit counter)
- Luminosity 3 bits barrel, 3 bits endcap

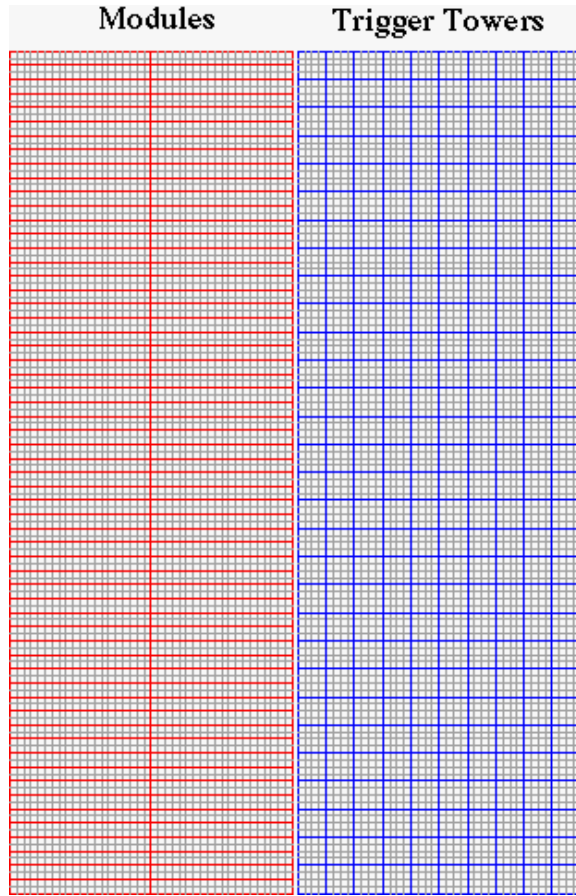


Figure I.2.4.1. Schematic drawing of STAR EMC showing the physical towers and the module boundaries (left) and the trigger tower boundaries (right). The vertical axis represents ϕ from 0 to 2π while the horizontal axis depicts η from -1 to 1 for each frame.

- ($E_t > 3$ thresholds for barrel and endcap separately)
- Jet patch (1.0,0.8) > 3 thresholds; 3x2 bits (2 bit counters)

I.2.6 Upgrade Options

The design of the EMC has left open several upgrade options. None of these will be addressed in any detail in this document, but they will be briefly outlined here for completeness.

1. The Pre-shower detector option

The primary tools for electromagnetic shower identification in the EMC are the shower maximum detector and the calorimeter tower response compared to momentum from tracking. The present design has been crafted to match the requirements of the EMC physics program. There are some aspects of the program that would be greatly enhanced by the improved electron – hadron separation that would be afforded by a pre-shower detector. In particular the identification of low energy electrons would greatly expand the J-Psi capability of STAR. This would have very significant impact on the reach of J/Psi as a diagnostic tool of Au+Au collisions, for example. The current EMC design includes a second set of read out fibers for the first layer of the calorimeter stack built into the detector and routed to the PMT boses on the magnet. An upgrade that would provide multi-anode photo tubes for these fibers and read-out electronics would be required to implement the pre-shower detector option.

2. SMD level – 0 trigger

The Shower Maximum Detector is designed with the provision to read out the wire signal from an eta-phi patch of 1.0 x 0.1. An amplifier-discriminator or ADC system could be built as an upgrade with the addition of the appropriate number of STAR trigger processor modules (DSM's) to permit the use of SMD primitives in the level 0 trigger as an enhancement to the direct photon trigger.

3. EMC Level – 2 Trigger

Overlapping Jet trigger towers of eta-phi = 0.8x0.8 would enhance jet threshold resolution beyond that achieved at level-0 with non-overlapping patches. It is prohibitively expensive to compute these patches in the level-0 trigger processors. As an upgrade, we have preserved the option to place the 0.2x0.2 EMC trigger tower data into a memory for use by processors that could be added to the STAR trigger system at level-2. A very early level-2 decision could have a significantly impact in pp running at RHIC's proposed upgraded luminosity.

Likewise, we have preserved the option to read out full resolution EMC and SMD data to a level-2 processor farm that would allow photon isolation cuts and other cuts utilizing correlation of the EMC and SMD to be made at the trigger level.